Coastal acid sulfate soil processes in Barker Inlet, South Australia

Doctor of Philosophy

The University of Adelaide

School of Earth and Environmental Sciences

Brett P. Thomas

September 2010

Chapter Eleven

11. Micromorphology – a comparison of soil processes within contrasting coastal acid sulfate soil landscapes

Integrating soil micromorphological research with pedo-geomorphic studies is a powerful tool to help understand complex contemporary and relict processes in soils from evidence at a finer (sub mm) scale (Brewer and Sleeman 1988; Fitzpatrick 1984; Rabenhorst and Lindbo 1998; Stoops 2003). The literature associated with soil micromorphological and pedo-geomorphic studies of coastal acid sulfate soil landscapes is not extensive for areas with Mediterranean type climates, especially in Australia. However, SEM studies on coastal acid sulfate soil in sub-tropical climates in eastern Australia has been conducted by Bush and Sullivan (1999) and Fitzpatrick *et al.* (1993b).

Soil micromorphological features (i.e. Fe oxides coatings, types of organic matter and aluminosilicates, porosity and the distribution of pyrite and monosulfides) can improve understanding of acid sulfate soil processes, (e.g. estimating oxidation rates and acidification potential of sulfidic materials), which is critical for managing acid sulfate soils.

In this chapter, soil micromorphology and mineralogy, by means of light microscopy, scanning electron microscopy (SEM), and X-ray diffraction (XRD) are used to determine mineral weathering pathways and mechanisms under changing hydrological, physical and biogeochemical conditions in soils from the two study sites with contrasting coastal environments:

i) an intertidal mangrove forest at St Kilda (profiles 600 and 2610), and

ii) a former supratidal samphire area at Gillman that was drained in 1935 causing sulfuric materials to develop (profile BG 11).

11.1. Introduction

The first micromorphological observations of acid sulfate soils were those of van Dam and Pons (1973) on acid sulfate soils from Thailand, Nigeria and the Netherlands, focusing on the micromorphology and occurrence of pyrites. The authors distinguished between primary pyrites, scattered in the matrix or in syn-sedimentary organic matter (like diatoms or foraminifers) and secondary pyrite associated with organic matter. The micromorphology of primary pyrite structures have also been used as a proxy to identify a variety of redox controlled cyclic transitions and depositional environments (Boesen and Postma 1988; Raiswell and Berner 1985; Wilkin *et al.* 1996). The rate of pyrite oxidation can be influenced by pyrite morphology, its distribution and the chemical conditions within sediments (Bronswijk *et al.* 1995; Bush and Sullivan 1999; Luther *et al.* 1986; McKibben and Barnes 1986; Nordstrom and Southam 1997). The morphology, texture, composition and distribution of pyrite oxidation products, such as jarosite can also provide clues to the chemical conditions within coastal (Poch *et al.* 2009) and inland (Fitzpatrick *et al.* 1996b; Wallace 2009) environments.

In modern euxenic environments, the mean framboid diameters are generally smaller (below 10 μm) and have a narrower size range than for oxic and dysoxic environments Wilkin *et al.* (1996). However, given the dynamics of these coastal systems where sediments are subject to daily and seasonally oscillating environmental determinants, caution should be employed when using pyrite structure morphologies as a proxy for interpreting the redox conditions of different depositional environments (Roychoudhury *et al.* 2003). Secondary pyrite often occurs as clusters of pyrite framboids, 20 to 50 μm in diameter, or scattered framboids when the organic matter decays (van Dam and Pons 1973). Oxidation proceeds from crack walls (planar voids) into the peds, with the first oxidation products being poorly crystalline iron oxyhydroxides that precipitate along ped walls, impregnating the matrix and producing iron hypocoatings (Bullock *et al.* 1985; van Dam and Pons 1973).

van Dam and Pons (1973) noted that iron oxidation products are usually poorly crystalline iron oxyhydroxides, but can also include crystalline goethite and hematite whenever a seasonal dry period permits dehydration of soils. Whenever calcium was available, gypsum precipitated in pores as pseudo-rhombohedral crystal infillings or coatings, or as hypo- or quasicoatings in pores (Bullock *et al.* 1985; van Dam and Pons

1973). When calcium is provided by inundation waters, gypsum precipitates above jarosite layers. Cryptocrystalline silica (opal) can precipitate proximal to pyrite, and it is believed to be derived from weathering of layer aluminosilicate minerals. Miedema *et al.* (1974) observed the process of oxidation of pyrite from outer to the inside of the framboids, noting the first products are poorly crystalline iron oxyhydroxide hypocoatings, and pseudomorphs after pyrite framboids, which sometimes have a remnant nucleus of pyrite. In non-calcareous environments, if pyrite oxidation proceeds, the pH decreases enough (i.e. pH < 4) so that Fe-oxides transform to jarosite. Jarosite can occur immediately adjacent to Fe-oxides in similar forms: pseudomorphs after framboids (e.g. in voids) or as hypocoatings and quasicoatings, the latter sometimes associated with Fe-hypocoatings. The transformation of jarosite to Fe-oxide is caused by iron hydrolysis after dissolution of jarosite when H^+ is leached. The transformation releases Fe^{3+} at relatively high pH and therefore the Fe oxides are immobile and precipitate near the jarosite. When the oxidation is faster, the intermediate stage of Fe-oxide formation does not occur and jarosite is formed immediately after oxidation of pyrite (Miedema *et al.* 1974). In calcareous environments, gypsum precipitates as coatings and infillings in pores (Miedema *et al.* 1974). The distinction between calcareous and non-calcareous environments is indicated by more rapid precipitation of Fe oxides in calcareous soils. Therefore, Fe-hypocoatings are a redoximorphic feature in well-buffered soils (Miedema *et al.* 1974), and jarosite are a redoximorphic feature in non-calcareous soils.

Studies describing the distribution, formation and chemical and physical properties of acid sulfate soils in Australia have mainly focused on sub-tropical to tropical coastal acid sulfate soils in New South Whales (NSW) and Queensland (Qld) (Ahern *et al.* 1998; Bowman 1993; Bush and Sullivan 1996; 1998; Johnston *et al.* 2009b; Lin and Melville 1992; Sammut *et al.* 1995; Sammut *et al.* 1994; White and Melville 1993; White *et al.* 1993; White *et al.* 1997; Willett and Walker 1982). Bush and Sullivan (1999) described the morphology, distribution and composition of pyrite in Holocene estuarine sediments from the north coast of NSW. According to their observations, all pyrite (i.e. framboids associated with organic remnants and scattered pyrite in the matrix) was formed *in situ*, due to either microbiological activity, dislodgement from framboids or formation from diffusion. Bush and Sullivan (1999) emphasised the importance of soil microscopic features (i.e. coatings of Fe monosulfides, organic matter

or aluminosilicates, porosity and the distribution of pyrite) as a tool for underpinning the understanding of acid sulfate soil processes (e.g. estimating oxidation rates and acidification potential of sulfidic materials) which is critical in managing acid sulfate soils. However, few published studies (Fitzpatrick *et al.* 1996a; Fitzpatrick *et al.* 1993b; Poch *et al.* 2004; Poch *et al.* 2009; Thomas and Fitzpatrick 2006b; Thomas *et al.* 2004b) have involved coastal acid sulfate soils from southern Australia with a Mediterranean type climate (i.e. characterised by extended hot, dry summers and cool, wet winters). Climate controlled acid sulfate soil processes, analogues to Mediterranean type climates may also occur in tropical regions of northern Australia (e.g. Northern Territory and Western Australia), during late dry-season prior to the mid- to late- wet-season (Melville 2010). Hence, an objective of this chapter is to provide more detailed micromorphological and mineralogical descriptions and new interpretations of soil processes occurring in Australian coastal acid sulfate soils.

11.2. Materials and methods

Soil and mineral samples from four soil profiles; two from the St Kilda study site (refer to Figure 5-1 and Figure 8-5) and 2 profiles from the Gillman study site (refer to Figure 6-1 and Figure 5-3) were analysed for mineralogy and micromorphology using XRD, SEM and petrology (light microscopy). These four soil profiles were selected to represent a range of physiographic categories which included: **(i)** intertidal, sulfidic mangrove soil under strong tidal influences (profile 2610), **(ii)** intertidal, sulfidic mangrove soil under moderate tidal influences (profile 600), **(iii)** drained, sulfuric, sulfidic, non-tidal (former supratidal) soil (profile BG 11), and **(iv)** salt efflorescence on the exposed face of soil profile pits.

Sample collection and preparation

Horizontal and vertical thin sections were made from undisturbed soil blocks of surface and subsurface soil horizons using the method of Salins and Ringrose-Voase (1994). Blocks were collected from two depth intervals in soil profiles 600 (0-12 cm and 12-32 cm) and 2610 (0-8 cm and 8-30 cm). Undisturbed soil blocks were collected using Brewer tins (Brewer 1964) from five depth intervals from soil profile BG 11 (2-15 cm, 35-48 cm, 50-65 cm, 75-88 cm, 92-108 cm and 146-161 cm) (Figure 11-1). The study and description of thin sections followed guidelines and terminology of Stoops (2003).

SEM and EDX studies were made on carbon coated polished blocks, thin sections and rough surfaced soil fragments glued onto stubs. Secondary electrons (SE) were used to collect high resolution images as they are emitted from the sample's surface atoms and relate to the samples morphology. Back-scattered electrons (BSE) are electrons that have an energy close to that of the electrons in the incident beam of the SEM. The intensity of back-scatter electrons is positively correlated with the mean atomic number of a sample. Therefore, the intensity variations in back-scattered electron images relates to different chemical phases in the sample. The relatively high energy of back-scattered electrons means that they can be ejected from deep (several microns) within a sample and therefore BSE images show less surface detail than secondary electron images. Powder X-ray diffraction (XRD) investigations used to determine mineralogy were made on finely ground samples using a Philips PW1800 microprocessor-controlled diffractometer using Co K-alpha radiation.

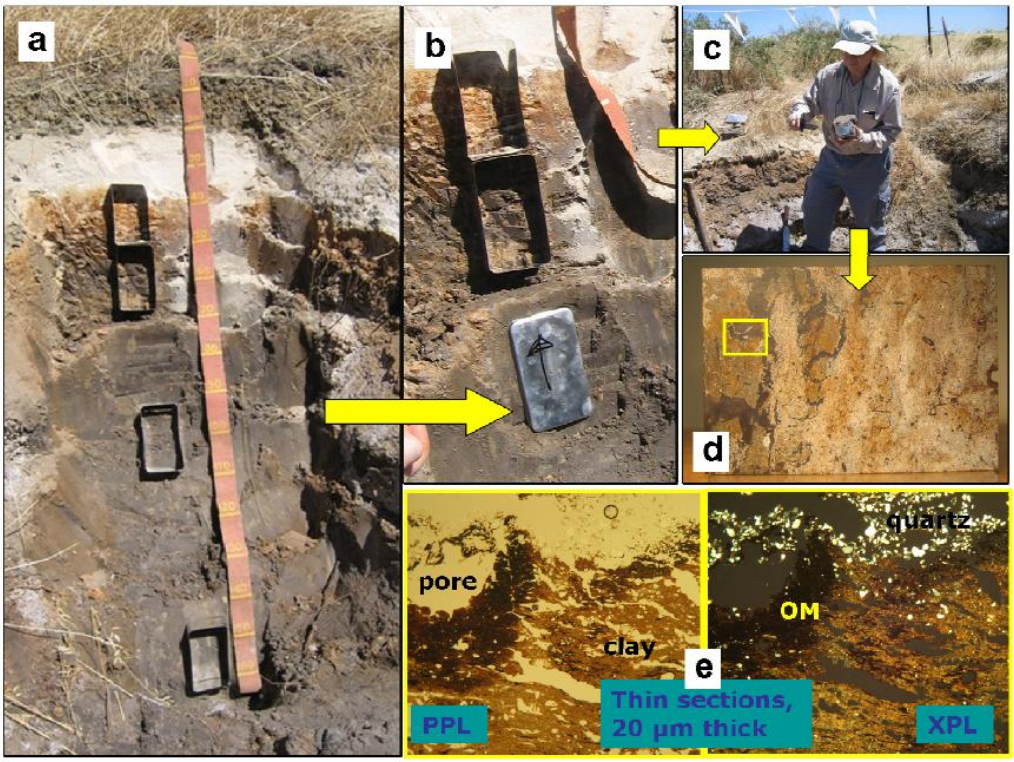

Figure 11-1 (a) soil profile BG 11 at the Gillman study site with Brewer tins placed on the profile face in preparation for collecting undisturbed samples for thin section preparation (January 2004). (b) and (c) soil blocks were orientated so vertical and horizontal blocks could be prepared for soil samples from 5 depth intervals (2-15 cm, 35-48 cm, 50-65 cm, 75-88 cm, 92-108 cm and 146-161 cm). (d) following impregnation with epoxy resin, the blocks were cut to size and one surface polished. (e) a thin section was produced from an area on each block (e.g. indicated by the yellow square on (d)) and viewed with a microscope under plane polarised light (PPL) and crossed-polars (XPL). The uncovered thin section samples were also viewed under SEM.

11.3. Macromorphology and soil classification

11.3.1. St Kilda study area

Soil profile 600 is located 250 m from the low tide mark at the seaward fringe of the mangrove forest (Figure 5-1) and only 2 m from soil profile BSK 1, at a similar position in the landscape (refer to Figure 5-2). Soil profile 2610 is located 50 m from the low tide mark at the seaward fringe of the mangrove forest (Figure 8-4) and was morphologically similar to soil profile BSK 4 (refer to Table 5-3). Both profiles, 600 and 2610, are permanently saturated and occur in intertidal areas with mangroves. Profile 2610 is more affected by tides due to its lower elevation and proximity to the coastline. Both profiles overlie unconsolidated Holocene coastal marine sediments consisting of saturated light grey, shelly and often silty or clayey sands of the St Kilda formation (Figure 8-4). Both profiles contain soil materials in layers that qualify as hyposulfidic and hypersulfidic material according to Sullivan *et al.* (2010).

A feature of these soils is that they contain horizons with different kinds of organic soil materials - as defined by the amount of rubbed fibre content (i.e. sapric has < 17% by volume rubbed fibre, hemic 17% > 40% rubbed fibre and fibric > 75% rubbed fibre) (Soil Survey Staff 2010). Hence organic horizons that contain predominantly sapric material have a large component of decomposed plant materials. This is used to determine the kind of organic materials when classifying soils according to (Soil Survey Staff 2010). Detailed macromorphological descriptions for profiles 600 and 2610 are given in Table 11-1. Profile 600 consists of a hemic Oe horizon overlying a sapric Oa horizon and classifies as a Typic Sulfiwassists (Soil Survey Staff 2010). Profile 2610 consists of a thin layers of hemic material at the near surface (Oe1) with thick underlying layers of sapric material (Oe2, Oe3 and Oa) and classifies as a Sulfic Haplowassists (Soil Survey Staff 2010). According to Isbell (2002) these profiles classify as a Hemic, Histic-Sulfidic, Intertidal Hydrosol (Profile 600), and a Sapric, Histic-Sulfidic, Intertidal Hydrosol (Profile 2610).

Table 11-1 Macromorphological descriptions of soil profiles.

Soil profile 600 • Map unit 10 – Mangrove woodland (young trees with adjacent samphire vegetation) • Classification: - Typic Sulfiwassists (Soil Survey Staff 2010) - Hemic, Histic-Sulfidic, Intertidal Hydrosol (Isbell 2002).		
Horizon (ID)	**Depth**	**Soil morphology**
Oe1	0-12 cm	Very dark brown (10YR2/2) peat; abundant very coarse roots and medium roots; hemic; gradual wavy boundary.
Oe2	12-32 cm	Black (5Y2.5/1) peat; many very coarse roots and medium roots; hemic; gradual wavy boundary.
Oe3/W1	32-48 cm	Black (5Y2.5/1) peat; common medium and coarse roots; hemic; slight H_2S smell; gradual wavy boundary.
Oe4/W2	48-55 cm	Black (5Y2.5/1) peat; common medium and coarse roots; hemic; moderate H_2S smell; gradual wavy boundary.
Oa5/W3	> 55 cm	Dark grey (5Y4/1) peaty loam; few medium roots; abundant shell, much broken: sapric.
Soil profile 2610 • Map unit 10 – Mangrove woodland (mature trees) • Classification: - Sulfic Haplowassists (Soil Survey Staff 2010) - Sapric, Histic-Sulfidic, Intertidal Hydrosol (Isbell 2002).		
Oe1	0-8 cm	Very dark brown (10YR2/2) peat; many coarse and medium roots; hemic; clear smooth boundary.
Oa2/W1	8-30 cm	Very dark greyish brown (10YR3/2) peat; many coarse and medium roots; sapric; moderate H_2S smell; gradual wavy boundary.
Oa3/W2	30-60 cm	Black (5Y2.5/1) peat; common medium and coarse roots; sapric; moderate strong H_2S smell; clear smooth boundary.
B	> 60cm	Abundant broken shell.

11.3.2. Gillman study area

Soil profiles BG 11 (map unit 6) and BG 15 (map unit 5) originally developed in a supratidal regime but tidal inundation was totally excluded in 1935 when a bund wall or levee bank was constructed that excluded water, resulting in the oxidation of sulfidic materials. The parent material occurs as several layers of lacustrine and tidal sediments deposited under mangrove and samphire vegetation on an old chenier dune systems that had limited acid neutralising capacity. Soil pH values less than 3 have developed in both profiles, with both profiles classify as Sulfuric, Salic Hydrosol (Isbell 2002) or Typic Sulfaquepts (Soil Survey Staff 2010). Detailed soil morphological descriptions and chemical properties, including acid sulfate soil characteristics, of both profiles were provided in Chapter 6. Main morphological features of profile BG 11 are summarised in Figure 11-15.

11.4. Micromorphology of intertidal soils at St Kilda

11.4.1. Surface layers with predominantly hemic material

Surface horizons (Oe) of profiles 600 and 2610 had high porosities (80%) and contained a high proportion of fibres. These layers were classified as hemic material because they contained moderately decomposed organic materials. In thin section many of the recognisable organic residues were anisotropic due to the preservation of cellulose (Figure 11-2 and Figure 11-3). These surface horizons, of both profiles 600 and 2610, contained a mixture of yellowish, amorphous organic matter (highly decomposed organic matter) and recognisable organic tissues and plant organs (less decomposed fibres). The latter had been altered to different degrees due to physical breakdown by fauna and chemical alteration, namely the blackening and formation of phlobaphene (Figure 11-2), a brown tannin product of oxidation that is very resistant to further decomposition (Bullock *et al.* 1985). At the near surface (Oe horizons), profile 2610 had more reddish, phlobaphene-rich organic residues than 600 (Figure 11-2 and Figure 11-3).

11.4.2. Subsurface layers with predominantly sapric material

Sapric materials contain less recognisable organic tissue (i.e. fibres) and more yellow, gelatinous, amorphous organic matter (Figure 11-2 and Figure 11-3). Lee and Manock (1974) also described a brown amorphous matrix in drained sapric material, with a strong aggregation in pellets due to faunal activity. In both profiles (600 and 2610), the sapric material had a lower porosity consisting of vesicles and vughs. This indicated the deeper horizons had a lower permeability than the near surface layers where hemic materials dominated. Layers with a higher content of hemic material had more conducting porosity due to more packing pores between plant fibres. The amorphous organic material was polymorphic (De Coninck *et al.* 1974) and was mixed with clay, and had a granular structure due to faunal activity (bioturbation). The amorphous material had a layered structure alternating with horizontal tissue and organ residues in the deeper horizons. In some areas cracks had formed, possibly due to desiccation of the sample, which possibly occurred during thin section preparation. Amorphous organic material had a yellowish colour with opaque, highly reflecting spots that occurred inside yellowish aggregates distant from the pore walls (Figure 11-2 and Figure 11-3). The coarse material consisted of fine muscovite flakes, diatoms and quartz grains. Some

blackened fibres were often found around tissue residues and appeared to have transformed to opaque intercalations in some instances (Figure 11-3). Less frequently the black material formed hypocoatings in the yellow organic groundmass. Microprobe analysis of the yellow organic groundmass indicated it had a higher clay content than in the black organic materials (Figure 11-3), which implies that the yellow organic materials were older and more stable. Another characteristic of the amorphous organic matter was that it had a high Na, Cl and S content, which indicated a capacity to retain these elements from seawater, as the sample was dried out.

11.4.3. Pyrite morphology in soils with contrasting tidal strengths

Pyrite framboids containing equi-granular crystals (which range from 20% to 5% of the framboids diameter) were identified within sulfidic material from both soil profile 600 and 2610 at St Kilda. Pyrite crystal forms were predominately cubic but octahedral forms also occurred. SEM images of sulfidic materials in profile 600 (from horizon Oe2) identified pyrite predominately occurring as tightly packed framboids, with a maximum diameter of 10 μm, occurring in close proximity to, or within, pores and organic matter (Figure 11-2). Singular pyrite cubes also occurred in profile 600, embedded and dispersed in organic matter, suggesting they formed *in situ,* after sedimentation (Bush and Sullivan 1999; Pons 1973). Pyrite framboids were generally larger in profile 2610, with a minimum diameter of 10 μm, with loosely packed framboids measuring over 50 μm in diameter. The larger pyrite framboids (up to 50 μm) were well formed in horizon Oa2 of profile 2610 and occurred as nests (clusters) of framboids up to 100 μm wide. Loosely packed and compact singular framboids also occurred in the organic groundmass (Figure 11-3). Single pyrite cubes occurring in profile 2610 ranged from 0.5 to 2 μm. Framboid diameters and crystal sizes varied more in profile 2610 (Figure 11-3) than in profile 600, and indicates profile 2610 was subject to more dynamic redox conditions (Bush and Sullivan 1999; Pons 1973). In both profiles 600 and 2610, framboids composed of cubic pyrite crystals occurred in close proximity to framboids made up of octahedral pyrite crystals, indicating that the variation in chemical conditions occurred on a micro-scale, and is supportive of *in situ* formation (Bush and Sullivan 1999; Pons 1973). Depositional formation of pyrite in these profiles would be less significant due to the limited time of tidal inundation, and less evident due to the high organic matter content of the groundmass and surface. Semi-quantitative EDX analysis of compact and dispersed framboids suggested they were composed predominantly of

pyrite (Fe_2S) but a few had EDX traces indicating monosulfides (FeS_{2-x}) also occurred in both profiles (Figure 11-4). The absence of very large framboids (i.e. non-dispersed framboids with a diameter greater than 50 µm) suggests that Fe was more limiting during pyrite formation in profile 600 (Roychoudhury *et al.* 2003; Sawlowicz 1993).

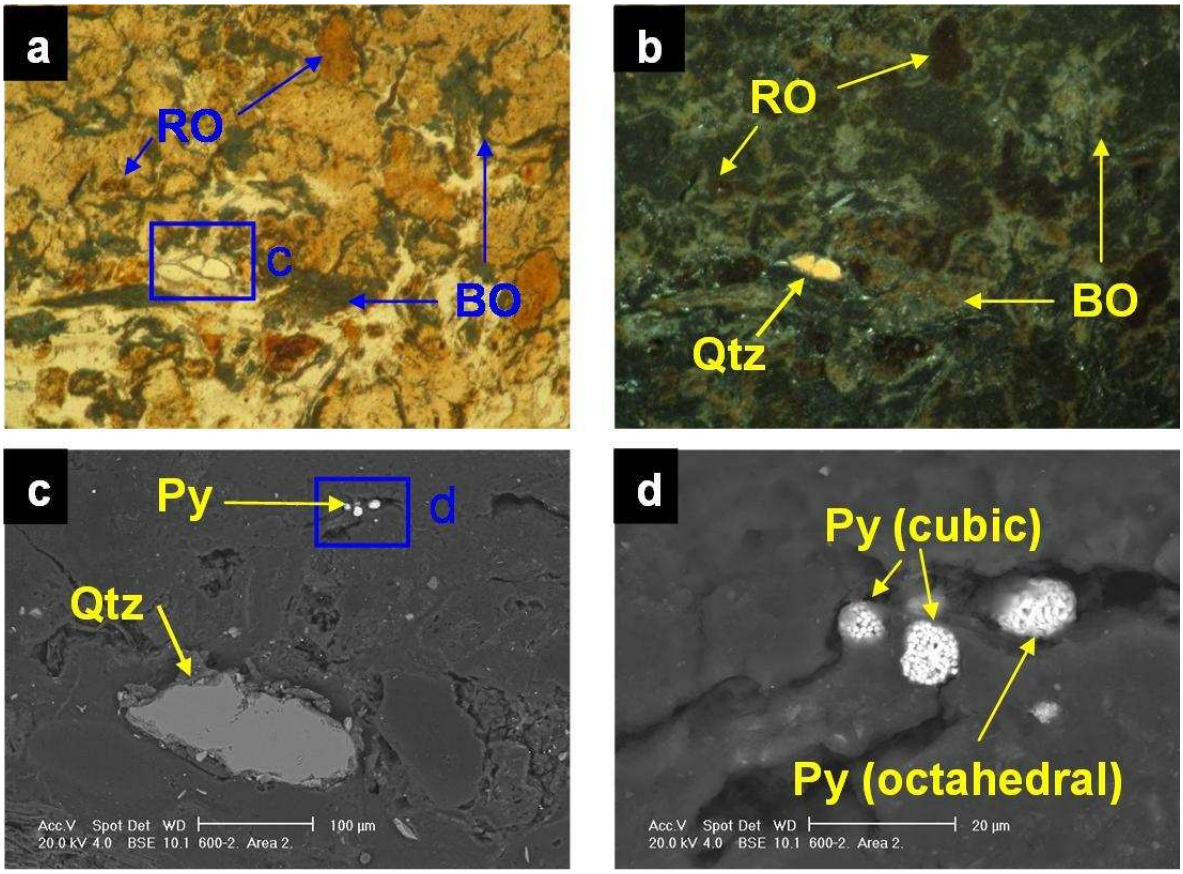

Figure 11-2 Profile 600. Thin section photographs using; (a) plane polarised light, (b) reflected light and (c and d) back-scatter electron (BSE) photomicrographs of polished resin-impregnated blocks from profile 600, horizon Oe2 (12-32 cm). (a) hemic material with blackened and red phlobaphene-rich tissue residues in a groundmass of yellow amorphous polymorphic organic matter. (b) same field of view as photograph (a). (c) enlargement of area (c) in image (a) showing 3 tightly packed pyrite framboids within porous blackened organic matter. (d) enlargement of area (d) in image (c) showing pyrite framboids. Two of the framboids are composed of cubic pyrite crystals while the third framboid (right) is composed of octahedral pyrite crystals (BO: black organic matter, RO: red organic matter, Py: pyrite). The field of view indicates scale and is 2.1 mm across in (a) and (b); 500µm across in (c) and 75µm across in (d).

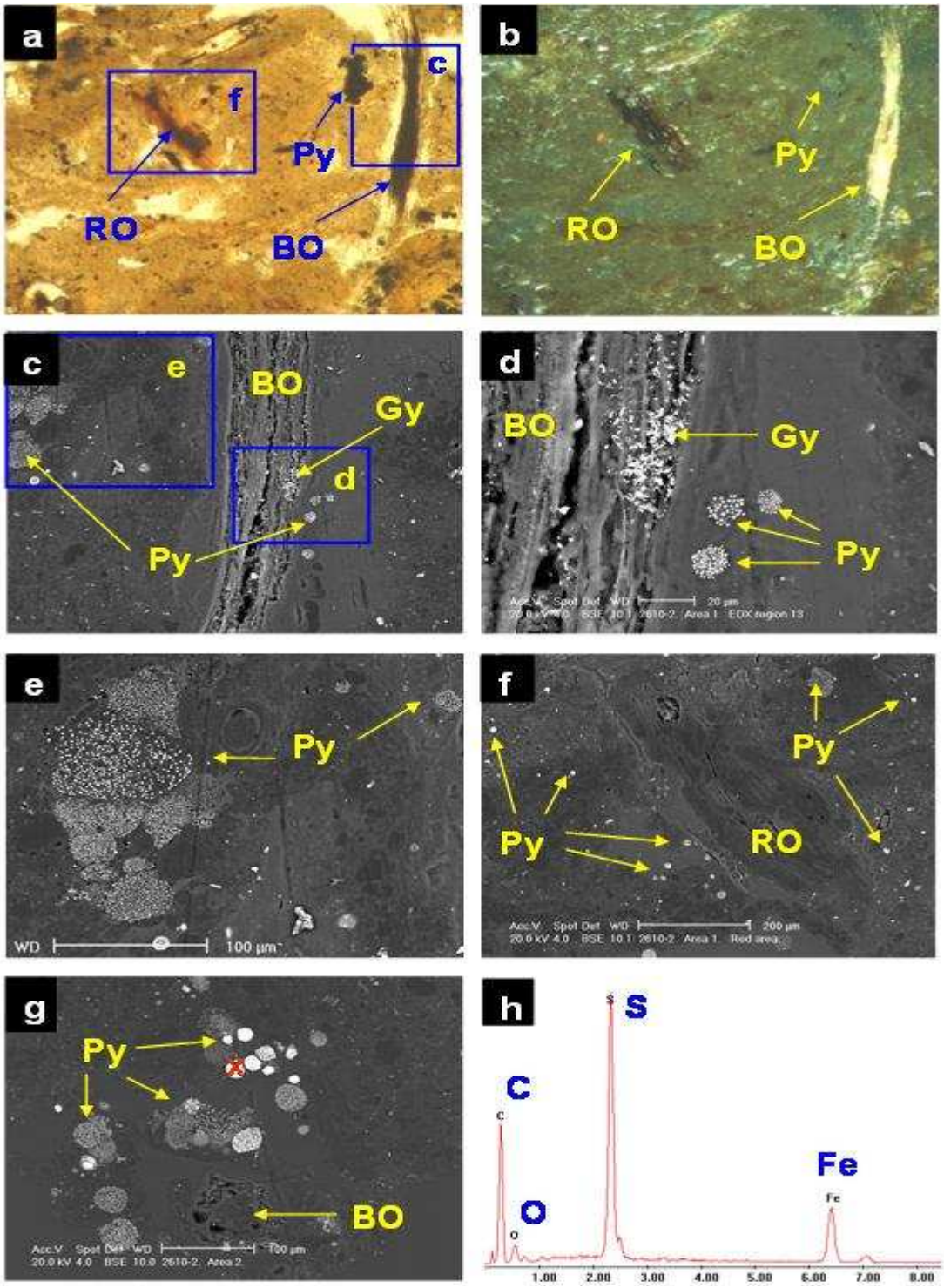

Figure 11-3 Profile 2610. Thin section photographs using; (a) plane polarised light, (b) reflected light and (c-f) back-scatter electron (BSE) photomicrographs of polished resin-impregnated blocks from, horizon Oa2 (8-30 cm). (a) sapric material with blackened and red phlobaphene-rich tissue residues in a groundmass of yellow amorphous polymorphic organic matter. A cluster of pyrite framboids is visible in the groundmass as an opaque cluster near porous blackened organic residue. (b) same field of view as photograph (a). (c) enlargement of area (c) in image (a) showing a cluster of loosely packed pyrite framboids and porous, elongate blackened organic matter. (d) gypsum crystals in blackened organic matter and pyrite framboids in groundmass. (e) enlargement of area (e) in image (c) showing a large cluster of loosely packed pyrite framboids within the groundmass. (f) enlargement of area (f) in image (a) shows pyrite framboids scattered throughout the groundmass. (BO: black organic matter, RO: red organic matter, Py: pyrite, Gy: gypsum). The field of view indicates scale and is 1500µm across in (a) and (b); 500µm across in (c); 150µm across in (d); 300µm across in (e); 800µm across in (f).

Fine gypsum crystals occur in the groundmass as nests of very fine prismatic crystals up to 2 μm in length within tissue residue in profile 2610 (Figure 11-3). The morphology of the prismatic gypsum crystals indicates they have formed *in situ* at very low pH values (Cody and Cody 1988). Tissue channels may provide sufficient aeration during low tides to enable oxidation of the pyrite or sulfide ions retained in the organic matter, lowering the pH and promoting *in situ* gypsum precipitation. Carey *et al.* (2002) observed euhedral, prismatic gypsum crystals up to 1 mm long in the roots of nursery-grown pine seedlings and attributed their formation to substrate dryness and excessive S supply through fertilisation, causing precipitation of gypsum in the root channel. Locally (micro-scale) acidic conditions, within the pore, were likely responsible for the elongate, prismatic crystal shape.

The occurrence of gypsum is indicative of pyrite oxidation, and was consistent with the large range of redox conditions (ranging from circum-neutral, weakly reducing to strongly reducing over one tidal cycle) measured *in situ* at soil profile BSK 4 that was located close to profile 2610 (Figure 8-27). The gypsum may also be an artefact of drying during thin section preparation, when buffering from seawater is negligible, but halite crystals would also be expected with desiccation, and were absent. The source of calcium is likely to be from detrital calcareous material or shell fragments. Pyrite oxidation is more limited in the sapric groundmass because the porosity of the amorphous organic material is low, consisting of non-conducting pores as vughs and vesicles. An anhedral grain of chalcopyrite was identified in a blackened tissue residue in the sulfidic material from profile 600. The chalcopyrite grain was likely contamination, a primary mineral grain from the crushed rock levee bank about 200 m north of profile 600 sample site (Figure 7-1). Some inclusions of detrital $CaCO_3$ were observed in plant tissue residues.

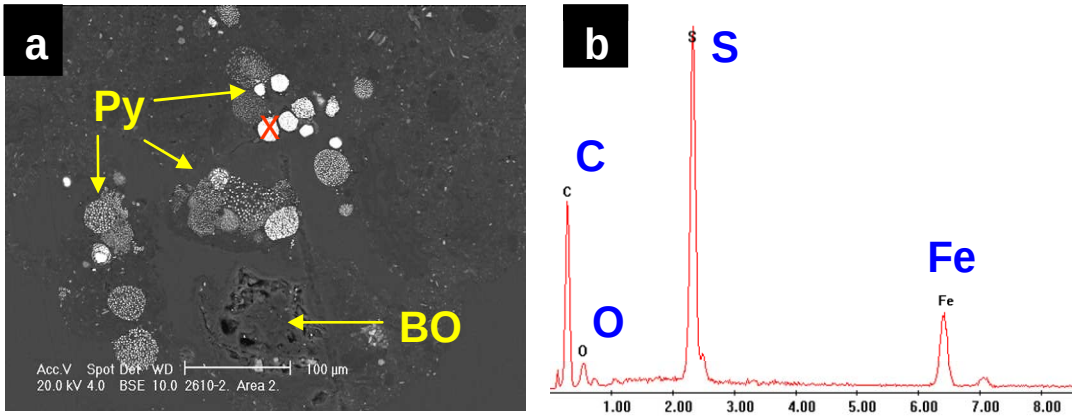

Figure 11-4 (a) SEM (BSE) from profile 2610 showing a cluster of loosely and tightly packed pyrite framboids within the groundmass adjacent to porous organic matter. (BO: black organic matter, Py: pyrite) (b) EDX analysis of framboids indicates they are composed of pyrite. The field of view indicates scale and is 500µm across.

Micromorphologically, profile 2610 shows better formation (semi-spheroidal framboids and euhedral crystals) of pyrite, a higher degree of decomposition of organic matter (less blackened residues) and a less conductive porosity than profile 600 (Figure 11-3). Tightly packed framboids were more common in profile 600 than in profile 2610 (Figure 11-2 and Figure 11-3). The pyrite morphologies observed were consistent with profile 600 having a more stable, strongly reduced biogeochemical environment than at profile 2160, with limited availability of reactive Fe (Wilkin *et al.* 1996). This was supported by the greater fluctuations in redox conditions occurring at profile 2610, measured across a tidal cycle (Figure 8-27 and Figure 8-28). Sulfur from sea water was the major source of S and S transformations resulted in the accumulation of organic S in the sapric material. Availability of Fe was probably the limiting factor for the formation of pyrite in these tidal environments. Framboids were mostly embedded within organic material and were more dispersed in the sapric material from profile 2610 than within hemic material from profile 600 (Figure 11-2 and Figure 11-3). The greater dispersal (disintegration) of the framboids in profile 2610 was likely related to physical disturbance (wave and tidal action, and bioturbation) being stronger within the finer, softer sapric materials. Another explanation may be that crystallisation of the pyrite crystals occurred *in situ* in the groundmass as dispersed framboids, which are a pre-cursor to tightly packed framboids (Sawlowicz 1993; Wilkin and Barnes 1997b; Wilkin *et al.* 1996). In this case it is less likely that the loosely packed pyrite grains will become tightly packed framboids due to the crystals being embedded within organic matter and due to the dynamic nature of the chemical and physical environment. The co-existence

of contrasting sulfide compositions, pyrite structures and sulfide oxidation products were influenced by the existence of microcosms created by variations in root density, texture and organic matter types. Variations in conductive porosity dictate the soil's susceptibility to redox condition changes induced by movement of water through the soil during tidal flooding and flushing. Detailed micromorphological descriptions are found in Table 11-2.

11.5. Micromorphology of a drained coastal soil at Gillman

Soil profile BG 11 classified as a Sulfuric, Salic Hydrosol (Isbell 2002) and Typic Sulfaquepts (Soil Survey Staff 2010). Profile BG 11 shows the presence of five lithological discontinuities and the processes that have acted on them: waterlogging followed by desiccation of the swamp. Profile BG 11 contains sulfuric material with bright yellow jarosite mottles above hypersulfidic and hyposulfidic materials. A detailed description profile BG 11 soil morphology is provided in Table 6-3. The main macro- and micromorphological features of profile BG 11 are summarised in Figure 11-15, and detailed micromorphological descriptions are presented in Table 11-3.

11.5.1. Oxidation of hyposulfidic materials

The near surface horizons (Oe and A) had a well developed crumb structure, formed by a mixture of calcareous and non-calcareous aggregates that were partly layered, with horizontal planar and lozenge-shaped (lenticular) voids, showing a porostriated and granostriated b-fabric, indicating displacive crystallization (Figure 11-5). Capillary rise may have initially supplied calcium enriched groundwater to clay rich layers allowing gypsum and halite to precipitate within the clay groundmass. The lenticular voids can be attributed to gypsum lenses formed in water-saturated conditions and dissolved after the soil profile was drained. The A horizon also contained nodules of Fe-oxides in the aggregates, not related to pores, similar to the underlying 2Ey2 horizon. The Fe-oxides replaced pyrite framboids that formed under past anaerobic conditions in pores and the groundmass. Following drainage of the profile, pyrite rapidly oxidised in a calcareous environment allowing the *in situ* precipitation of Fe-oxides forming pseudomorphs after pyrite, a process also observed in coastal and inland acid sulfate soil environments by Miedema *et al.* (1974) and Wallace (2009) respectively. The soil structure was altered

by biological activity (introduction of pasture grasses) and ped formation. Jarosite was absent because of the presence of detrital $CaCO_3$. Micro scale occurrences of jarosite may have formed but were subsequently leached, or converted to Fe-oxides.

The two underlying E horizons consisted of sands that lack organic matter except near the lower boundary (horizon 2Ey2), where there were frequent iron coatings and hypocoatings near plant remains (Figure 11-5). Iron nodules were clay-coated pseudomorphs of pyrite framboids (Figure 11-6) which originated from fast pyrite oxidation in a calcareous environment, similar to the overlying Oe and A horizons (Figure 11-6).

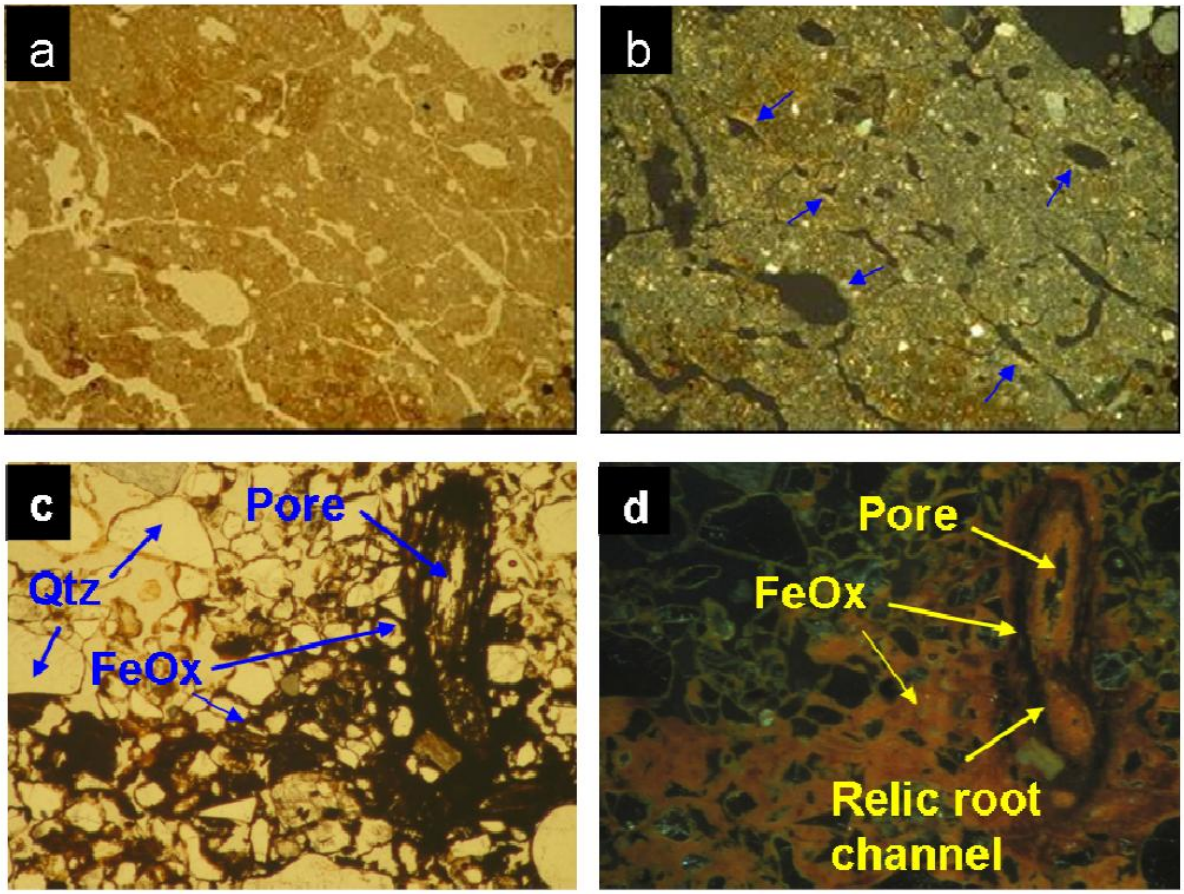

Figure 11-5 Thin section photographs from soil profile BG 11 samples using: plane polarised light (a), (c) and crossed-polars (b) and reflected light (d). (a) horizon A with lenticular voids, showing granostriation, visible under (b) crossed polars as light areas in the groundmass (indicated by arrows). (c) horizon 2Ey2 showing a pore (root channel) surrounded by Fe oxide. (d) same field of view as photograph (c). The field of view indicates scale and is 5.5 mm across in (a) and (b); 3.2 mm across in (c) and (d).

The most notable pedo-features within the 2Ey2 horizon were the ones related to oxidation of pyrite; as iron oxide pseudomorphs and coatings, frequent gypsum lenses in the clay matrix, and jarosite coatings (Figure 11-5). The predominantly clay 3Bty1

horizon had a similar structure to the Oe horizon: layered clays alternating with organic intercalations, lenticular voids and porostriation. The boundary with the overlying sands (horizon 2Ey2) was abrupt and therefore precludes illuvial origin of the clays in this layer. The top of horizon 3Bty1 contained a discontinuous lens of decalcifying shells (Figure 11-15). The horizontal structure of the clays and the abundance of well preserved organic matter were likely due to sedimentation under wet, strongly reduced, conditions that favoured pyrite formation. When the water table lowered following tidal exclusion, Fe-oxide pseudomorphs of pyrite framboids formed as the pyrite oxidised. Due to the lower permeability of the clays, a perched watertable may have developed on top of the layer to slow the oxidation rate post-bunding, or cause seasonal variations in redox conditions. Slower oxidation rates of pyrite may be partially responsible for producing the pitted textures on the exposed crystal faces of some pyrite framboids and larger octahedral pyrite crystals in horizon 2Ey2 (Figure 11-7). It is possible that an acidic, oxidised, micro-environment initially existed around some pyrite framboids that allowed jarosite to precipitate between the pyrite crystals to form a jarosite box-work texture. Similar weathering features in pyrite framboids have been described as honeycomb, box-work or weathering rinds (Fitzpatrick *et al.* 1996a; Skwarnecki *et al.* 2002; Wallace 2009).

On the basis of equilibrium stability, van Breemen (1982) concluded that jarosite should only form in oxidised environments (Eh > 400 mV) with pHs in the range of 2 to 4. The pH of the micro-environment was likely less than pH 4 but increased before the pyrite crystals were completely removed, allowing them (and any jarosite) to be replaced by iron oxides, preserving their morphology (Figure 11-7). The pitted crystal texture of pyrite framboids has also been described by Gong *et al.* (2007) who attributed the pitting to the direct pyritization (fossilisation) of clustered bacterial populations. It is more likely, in this case, that the pitted texture was related to oxidation of pyrite (dissolution) under acidic conditions. The texture may be enhanced by crystallographic (compositional) zoning of pyrite crystals that caused their cores to be preferentially oxidised. Similarly, crystallisation within pore waters with high dispersed clay contents may allow clay particles to be incorporated into the crystal structure of the pyrite grains (along the crystallographic growth axes) causing zoned weathering, analogous of dissolution textures in halite crystals. Clay-rich sediment would also provide stable

micro-environments. An alternative is that the texture is corrosion pits caused from contact leaching by iron oxidising bacteria (Tributsch 2001).

As soil pH became more acidic in the upper portion of profile BG 11, due to sulfide oxidation, shells in the 3Bty1 horizon began to dissolve and Ca was released allowing gypsum formation within juxtaposed layers (Figure 11-15). Gypsum crystal growth occurred on the surface of shells and within and adjacent to pore spaces. Little jarosite was present in the 3Bty1 horizon and was limited to micro-environments with less calcium availability, as the shell layers were discontinuous and irregular.

Organic matter and pH are two factors that control gypsum crystal morphology (Cody and Cody 1988; Jafarzadeh and Burnham 1992). Gypsum lenses and prisms generally form in neutral to basic pH in presence of organic matter and crystal shapes become flatter when crystallising from more acidic solutions (Cody and Cody 1988). Although some of the original gypsum crystals were dissolved, their crystal habit was evident by the abundance of lenticular and prismatic voids with porostriation (Figure 11-5). Due to the relatively high solubility of gypsum, several cycles of dissolution-precipitation likely occurred, since primary gypsum was formed. The short prismatic habit of the primary gypsum crystals in the upper part of the profile (0 to 50 cm) indicated they formed at near neutral pH (Cody and Cody 1988), due to a calcareous environment (Figure 11-15). Pseudohexagonal and lenticular gypsum crystals were found together in voids from hyposulfidic materials in horizon 3Bty1 and from sulfuric materials in horizon 4Bjy1 (Figure 11-9 and Figure 11-10) and indicate stages of formation under different chemical conditions. Changes in Ca saturation and pH of soil solutions had probably taken place, resulting in the different gypsum crystal shapes.

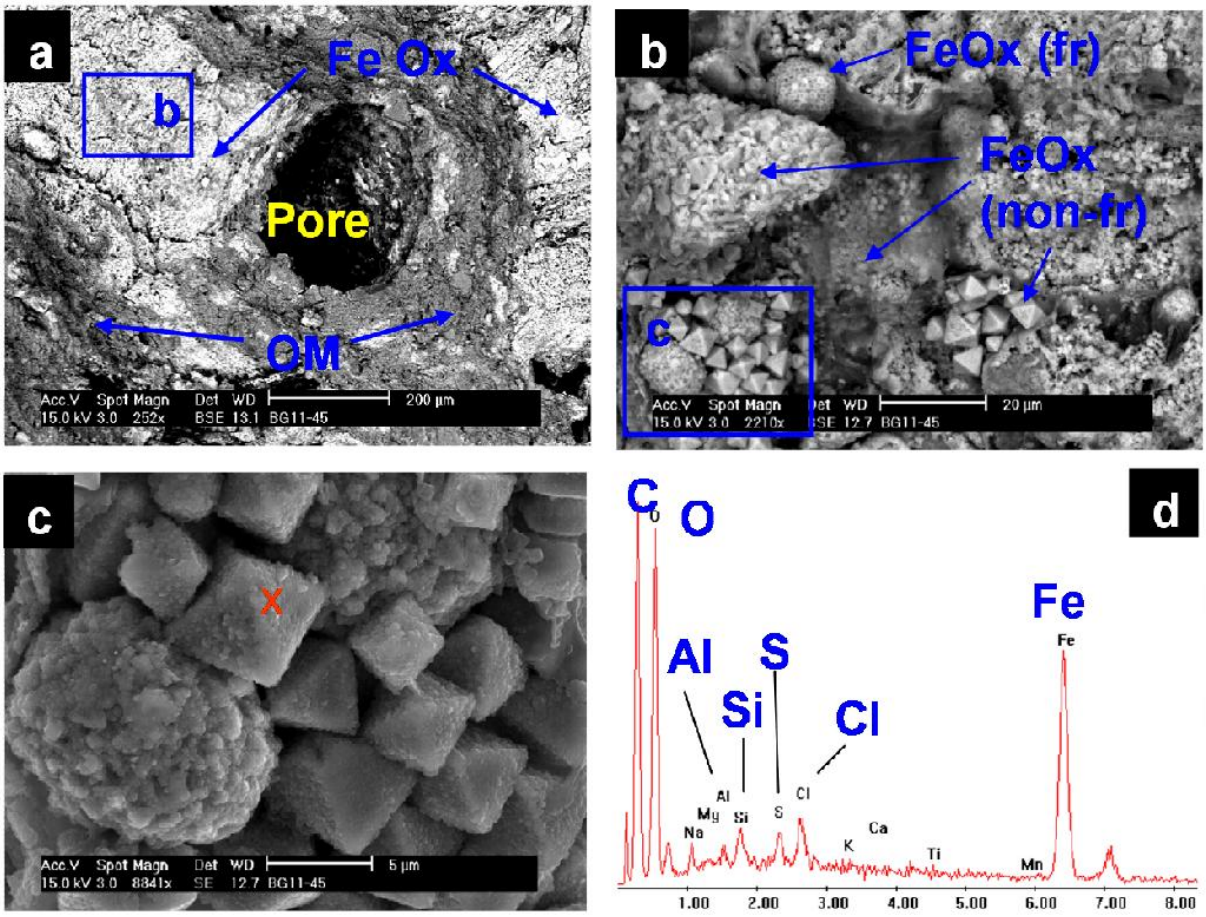

Figure 11-6 SEM photomicrographs of rough-surfaced soil samples (a-c) and EDX spectra (d) from profile BG 11. (a) horizon 2Ey2 showing a root channel surrounded by organic matter and Fe oxide. (b) enlargement of area (b) in image (a) showing framboidal Fe oxides and non-framboidal Fe oxides occurring as pseudomorphs after pyrite. (c) enlargement of area (c) in image (b) showing clay coating on large octahedral Fe oxide pseudomorphs and smaller framboidal pseudomorphs. (d) EDX spectra of large octahedral crystals (at site "X" in image (c)) indicating that they are composed of Fe oxide with clay coatings. The field of view indicates scale and is 1.2mm across in (a); 110µm across in (b); 25µm across in (c).

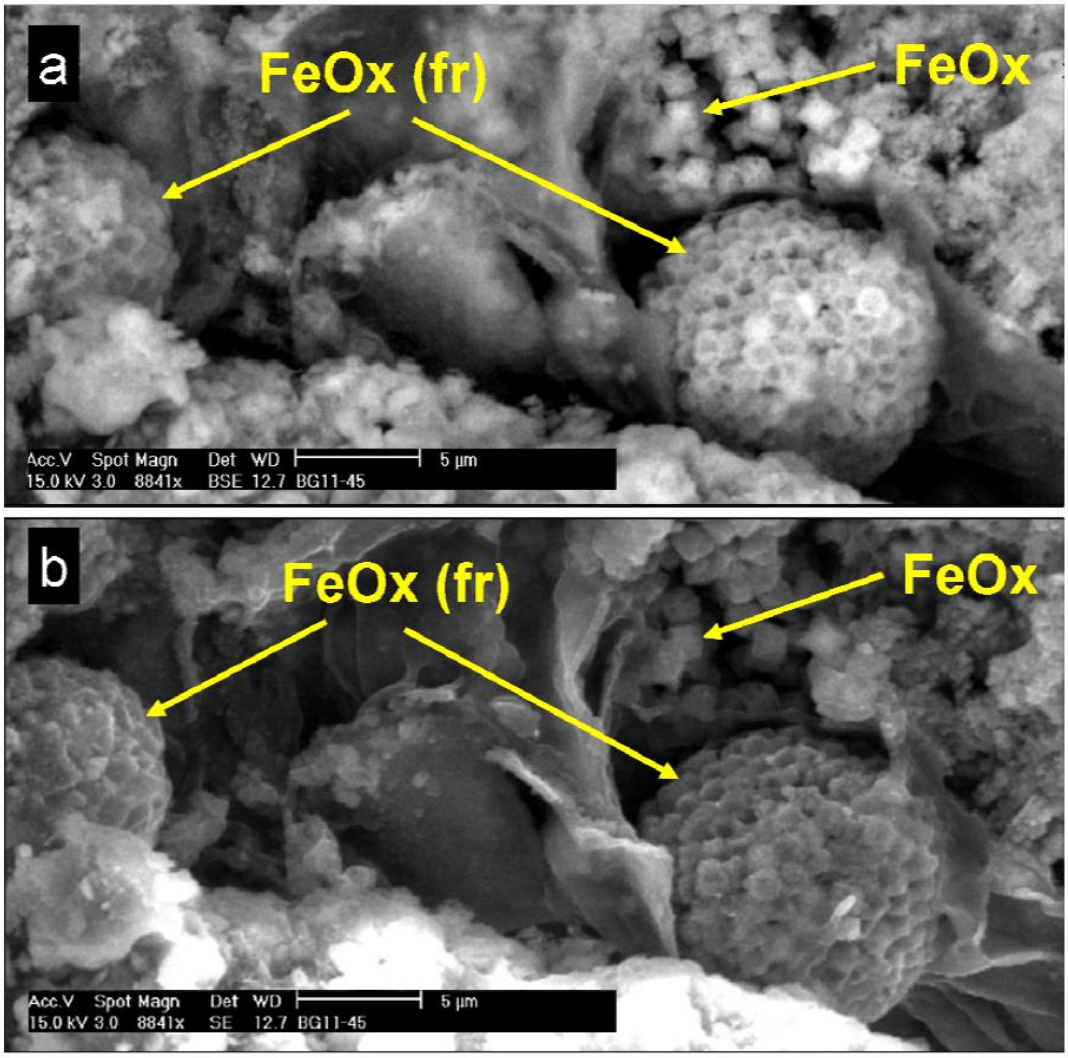

Figure 11-7 SEM photomicrographs ((a) BSE and (b) SE) of a rough-surfaced soil sample from profile BG 11, horizon 2Ey2 showing Fe oxide pseudomorphs of pyrite framboids with pitted faces on the outer crystals layer. The field of view indicates scale and is 50 µm across in (a) and (b).

Preserved pyrite crystals were identified by SEM analysis of soil samples from oxidising environments, in profiles BG 9 and BG 18 (Figure 6-1 and Figure 6-2). Pyrite was preserved (armored) in a number of ways (Figure 11-8): **(i)** by clay coatings on framboids, **(ii)** partial impregnation of framboids within large gypsum crystals, and **(iii)** inclusion of a pyrite framboids within halite crystals. It could be presumed that complete inclusion of pyrite crystals and framboids would also occur within these hyposulfidic materials, which has implications for characterisation of acid sulfate soil types by ageing as well as management.

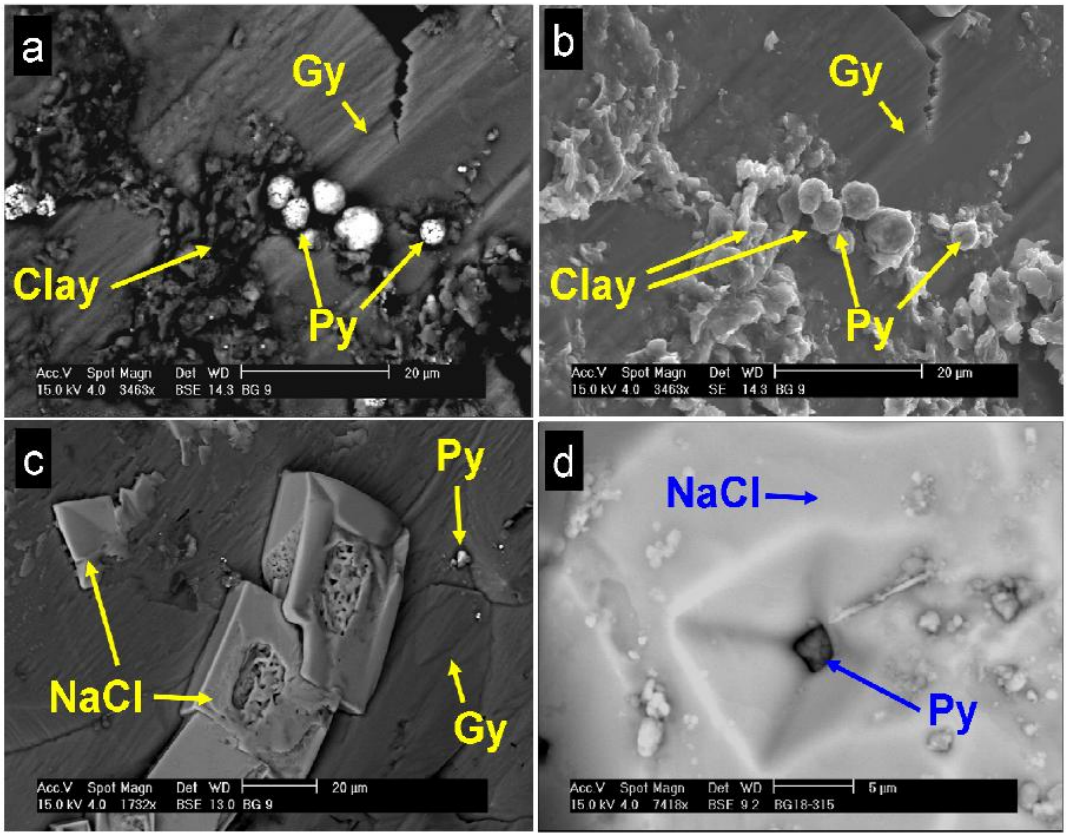

Figure 11-8 (a) BSE SEM and (b) SE SEM showing pyrite framboids preserved from oxidation by clay coatings and partial impregnation within gypsum crystals. (c) BSE SEM showing halite crystals precipitated at the same time or before gypsum and shows dissolution features in the cores of halite crystals. (d) BSE SEM showing near complete inclusion of a pyrite framboid within halite.

11.5.2. Oxidation of hypersulfidic materials

Horizon 4Bjy1 showed similar features to the 3Bty1 horizon, but in a much sandier matrix (Figure 11-15). Gypsum was generally lenticular, but also occurred as rhombohedral and pseudohexagonal crystal forms indicating precipitation under acidic and near neutral conditions respectively (Cody and Cody 1988). Gypsum also occurred as intercalations and infillings (Figure 11-9). Jarosite was identified around pores as coatings or hypocoatings in close proximity to gypsum (Figure 11-10). Fe-impregnating features occurred as quasicoatings or discontinuous coatings on the jarosite coatings. Jarosite coexists with gypsum since the gypsum may have been formed at the beginning of the oxidation process, when availability of calcium was higher. Jarosite became more abundant with depth (to about 110 cm from the surface) because: **(i)** water percolating through the soil profile precipitates gypsum removing Ca (buffering capacity) from the soil solution, allowing pH to fall sufficiently for jarosite to form and **(ii)** sulfide content of the soil profile increased with depth (refer to Chapter 6). The appearance of the

jarosite-impregnated groundmass with gypsum inclusions did not differ from the jarosite-free zones, suggesting that the jarosite hypo-coatings formed after gypsum had precipitated (Figure 11-10). According to Dam and Pons (1973), if oxidation is slow, sulfate and potassium migrate to pore walls and jarosite is formed as infillings, coatings or hypocoatings of very fine crystals in pores. Fe coatings (other than quasicoatings) can be explained by further hydrolysis of jarosite under a marked climatic, seasonal difference. In profile BG 11 the morphology of Fe oxide coatings indicated they originated directly from pyrite oxidation in organic residues (Dam and Pons 1973), which occurred adjacent to pores (Figure 11-10 and Figure 11-11). Oxidation of pyrite proximal to pores was likely rapid as iron oxides and jarosite precipitated at the site of pyrite occurrence (e.g. Figure 11-13). This is in agreement with the recent drainage history of the Gillman study area.

The underlying 4Bj2, 4Bjg3 and 4Bjg4 horizons contained a sandier matrix than horizon 4Bjy1 (Figure 11-15). Since gypsum has a similar birefringence as quartz its identification in these sand rich layers was difficult but it was less likely to occur in these layers since they lacked carbonate and because Ca was depleted from soil solution as it percolated down the acidic profile. Within these sulfuric materials, jarosite was the main product of pyrite oxidation as it predominantly occurred along coarse pores which were the first to aerate during drainage. Jarosite also occurred scattered within the groundmass as fine pseudo-cubes 0.5 μm in size (Figure 11-10 and Figure 11-13). The cubic morphology of primary jarosite (Figure 11-10) does not necessarily mean a pseudomorphic transformation from pyrite, since they can have the same crystal habit. EDX analyses indicated that these jarosite cubes contained more K than the soil matrix, and also that there was an excess of S, which suggested some pyrite was still present (Figure 11-10). Pyrite was confirmed to coexist with jarosite in thin section analysis of horizon 4Bjg5 (Figure 11-13), by XRD and by laboratory measurement of reduced inorganic sulfur (Chapter 6). Fe oxides were not as much related to the organic residues as in near surface horizons, pointing to a slower oxidation rate under acidic conditions that allowed Fe^{2+} to move further away from the original pyrite crystal site. NaCl salts had precipitated on quartz grains as needle-like crystals in some thin section samples and may be an artefact of drying the soil during thin section preparation (Figure 11-10).

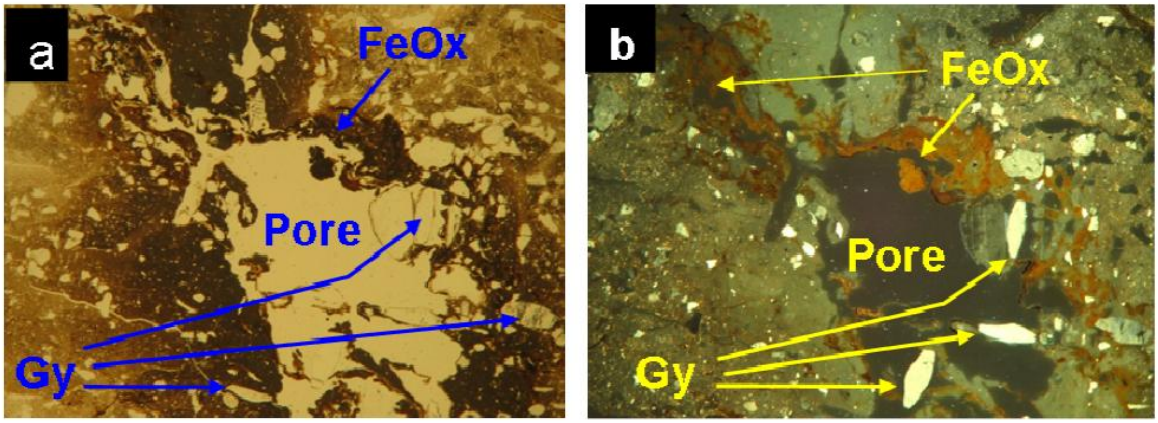

Figure 11-9 Thin section photographs from soil profile BG 11, horizon 4Bjy1 using; (a) plane polarised light and (b) reflected light. (a) showing a pore with loose discontinuous gypsum infilling and rhombohedral gypsum crystals and orange Fe coatings. (b) same field of view as photograph (a). The field of view indicates scale and is 6.5 mm across in (a) and (b).

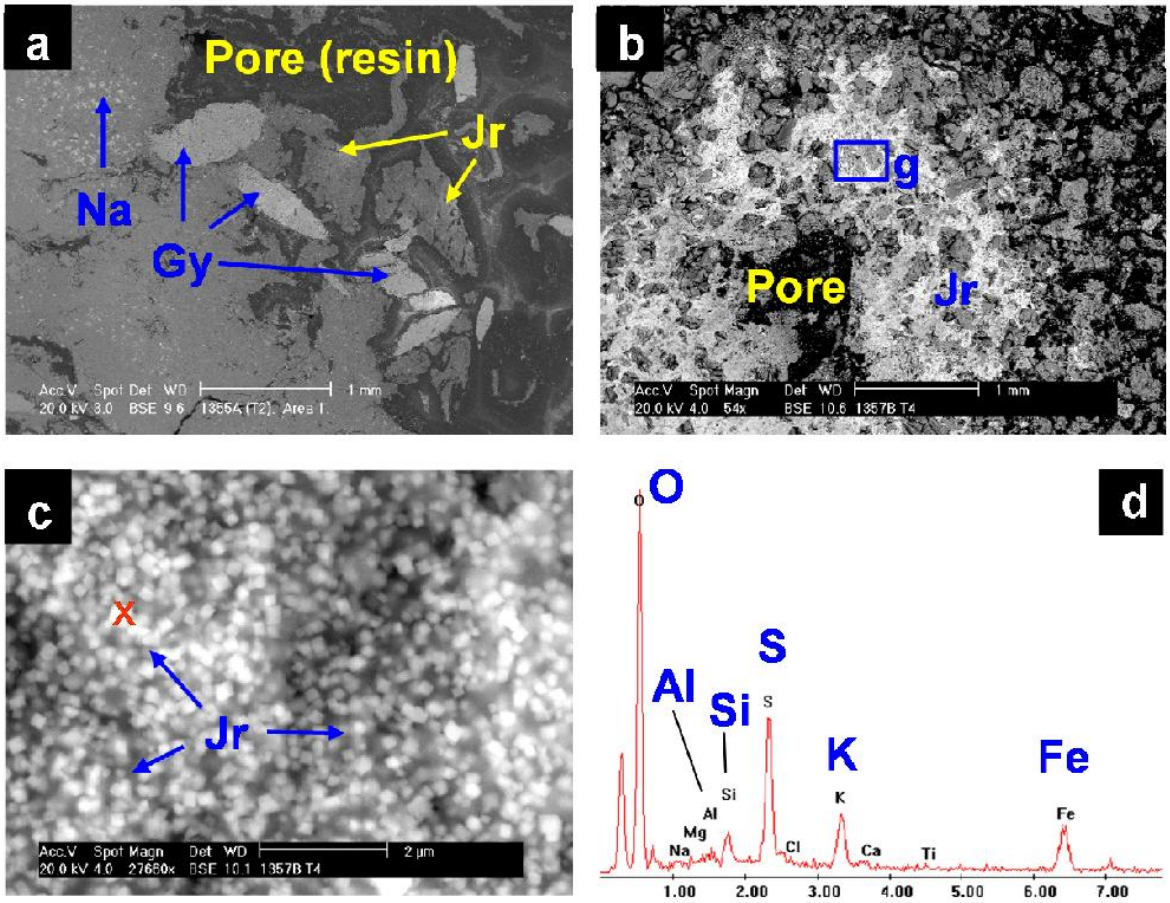

Figure 11-10 SEM photomicrographs of polished resin-impregnated blocks (a-c) and EDX spectra (d) from profile BG 11. (a) horizon 4Bj2 distribution of lenticular gypsum crystals. Halite and jarosite are dispersed in the groundmass. (b) horizon 4Bjg3 showing a circular cross-section of a pore surrounded by Fe oxide and jarosite. (c) enlargement of area (g) in image (b) showing jarosite cubes occurring in the groundmass surrounding a relic root channel. (d) EDX spectrum of the cubic crystals shown in image (c). (Gy: gypsum, Jr: jarosite, Na: sodium chloride salt). Field of view indicates scale and is 4.6mm in (a); 4.8mm in (b) and 9µm across in (c).

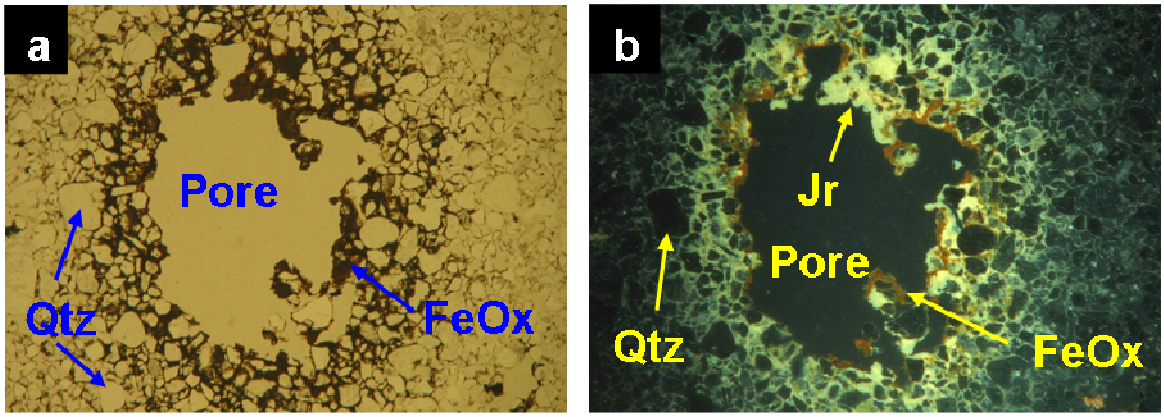

Figure 11-11 Thin section photographs from soil profile BG 11, horizon 4Bjg3 using; (a) plane polarised light and (b) reflected light. (a) circular cross section of a pore (root channel) surrounded by Fe oxide and jarosite. Jarosite (Jr) impregnated the quartz (Qtz) sand matrix and over-prints Fe oxide (FeOx). The field of view indicates scale and is 6.5 mm across in (a) and (b).

Spheroidal jarosite and Fe oxides were observed in salt crusts that had precipitated on the surface of sulfuric materials in profile BG 11. The jarosite spheroids likely formed by direct precipitation from jarosite-saturated pore waters rather than as pseudomorphs after pyrite framboids (Figure 11-12), due to their location on the surface of salt efflorescence samples. The Fe-oxide spheroids observed in the sample therefore are interpreted as pseudomorphs after jarosite spheroids, rather than after pyrite framboids.

Jarosite, starkeyite, pentahydrite, halite, gypsum and goethite were identified by XRD in the salt efflorescence samples collected from the face of profile BG 11 (Appendix G). EDX analysis of spheroids supported the XRD data (Appendix G). Although the jarosite and Fe oxide spheroids observed in the efflorescence sample were of comparable size to pyrite framboids identified in the soil profile, the spheroids had a closer morphology to jarosite spheroids described by Barróna *et al.* (2006), which formed as precipitates in a synthetic brine. The cracked surface texture of jarosite spheroids (also observed in the BSE image of Figure 11-12) was particularly noted by Barróna *et al.* (2006).

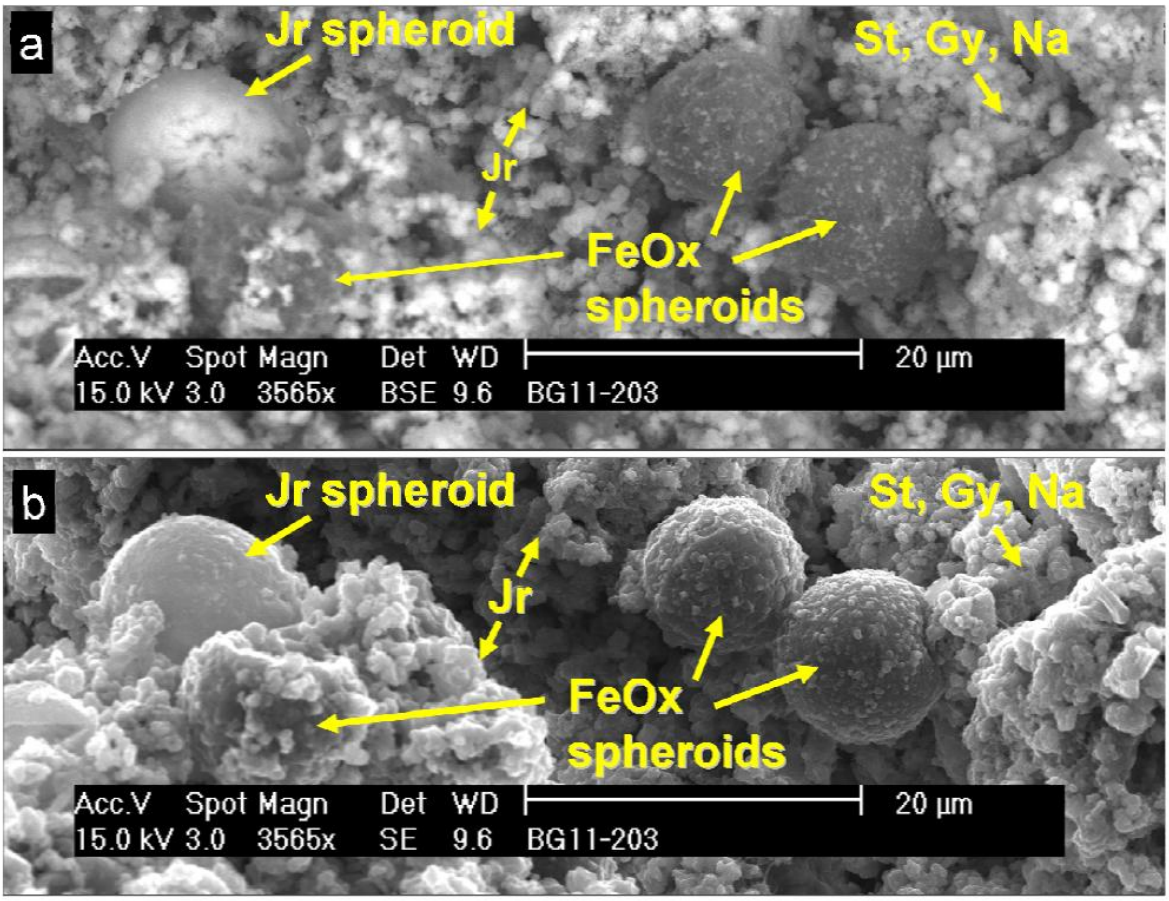

Figure 11-12 SEM photomicrographs (a) BSE and (b) SE showing a jarosite spheroid in a jarosite rich groundmass and two Fe-oxide spheroids that are likely pseudomorphs after jarosite. The sample was from salt efflorescence taken from the surface of sulfuric materials exposed in the pit face of profile BG 11. Jr: jarosite, FeOx: Fe oxide, St: Starkeyite, Gy: Gypsum, Na: halite.

11.5.3. Pyrite framboids occurring in sulfuric materials

Horizons 4Bjg5 and 4Bg6 classified as sulfuric material but pyrite was also present as scattered framboids in the groundmass and as aggregate nodules and clusters, often associated with organic material (hemic) forming pores (Figure 11-13 and Figure 11-14). Oxidation of pyrite was greatest proximal to large pores (relic mangrove pneumatophores), where jarosite had also formed (Figure 11-13). The soil pH was not buffered in these horizons due to the lack of calcite, and bicarbonate depletion. Amorphous silica could be present (van Dam and Pons 1973), derived from the weathering of clays, which become unstable at low pH. Very thin silica coatings were tentatively identified surrounding quartz grains (Figure 11-13 and Figure 11-14), as availability of weatherable clay increased with depth.

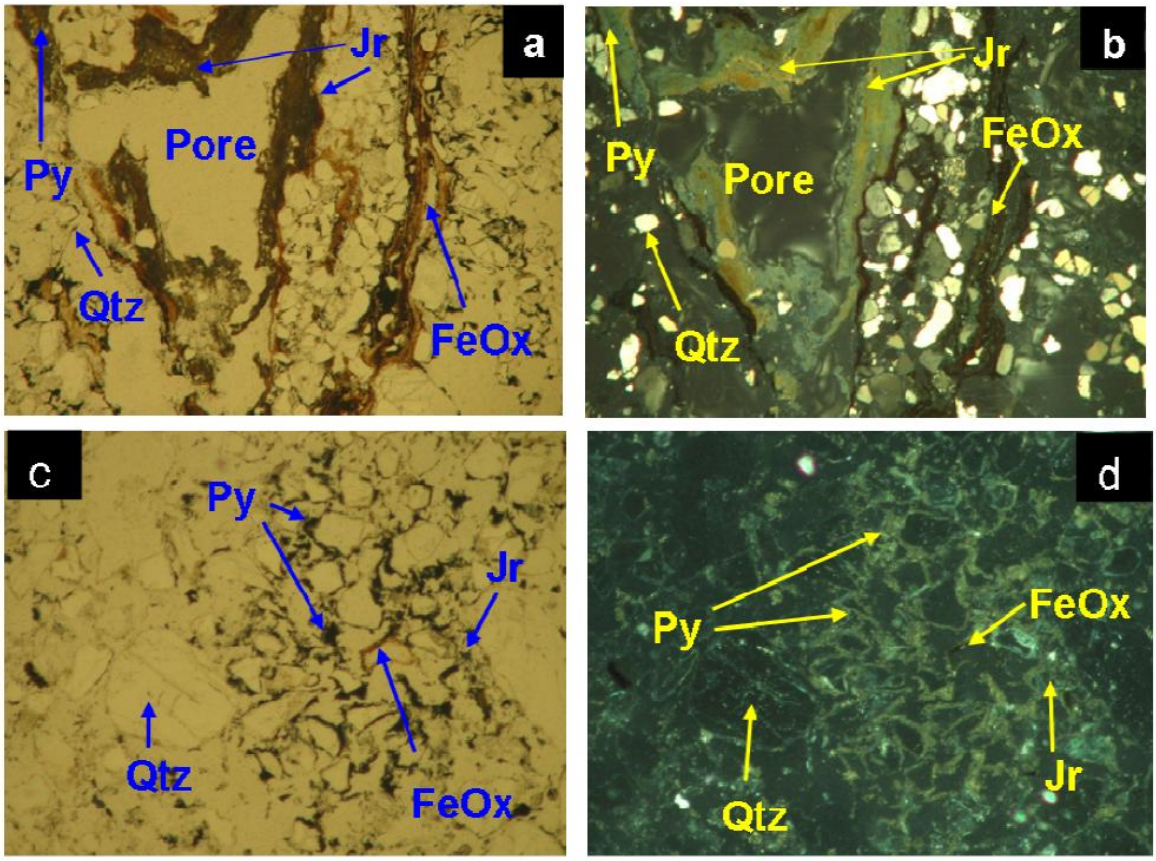

Figure 11-13 Thin section photographs from soil profile BG 11, horizon 4Bjg5 showing: (a) Fe hypo- and quasicoatings and (b) yellow jarosite hypocoating and pyrite quasicoating around a root channel (root tip) with organic residues in a quartz sand matrix. (c) and (d) aggregate nodule of pyrite framboids, partly transformed to jarosite. Note also that the light reflection around some quartz grains in (c) and (d) may correspond to silica coatings. There was no gypsum identified in horizon 4Bjg5. (FeOx: iron oxide, Jr: jarosite, Py: pyrite, Qtz: quartz). Frames (a) and (c) were viewed under plane polarised light, (b) under reflected light and (d) under crossed-polarisers. The field of view indicates scale and was 4.2 mm in (a) and (b), and 2.5 mm in (c) and (d).

In horizons 4Bjg5 and 4Bg6, pyrite crystals predominantly occurred as four morphological forms: **(i)** as small framboids (5 to 10 µm diameter) consisting of tightly packed cubic pyrite crystals measuring about 0.5 to 1.0 µm across, **(ii)** larger framboids (> 20 µm diameter) consisting of tightly packed cubic pyrite crystals measuring about 0.5 µm across, **(iii)** as large octahedral pyrite crystals measuring about 2 to 4 µm across that occurred as single grains in the groundmass and as clusters, and as **(iv)** small (0.5 µm across) single, cubic pyrite crystals occurring within the groundmass. The four forms of pyrite habits often occurred clustered together between sand grains (Figure 11-14), and were very similar to the pyrite forms (occurring as Fe-oxide pseudomorphs) observed in horizon 2Ey2 (Figure 11-6), although having a less obvious association with organic matter and voids. These varied morphologies are suggestive of multiple stages

of pyrite formation occurred under different redoximorphic conditions and stages in the geomorphic history of this profile. The small size of individual pyrite crystals that occur in the soil matrix, and form as an outer layer on some framboids (composed of larger crystals), supports the idea that some pyrite is formed and oxidised seasonally in the lower portion of the soil profile BG 11 (Figure 11-14). The strongly reducing redox conditions measured during wetter months within soils layers containing sulfuric material supports this inference (Chapter 8). Smaller pyrite crystals and framboids usually formed under more acidic soil conditions (Butler *et al.* 2000; Butler and Rickard 2000; Sawlowicz 1993; Schoonen and Barnes 1991a; Wilkin and Barnes 1997a; Wilkin and Barnes 1997b), suggesting that some pyrite oxidation within the profile had occurred, lowering the soil pH, prior to the formation of these secondary pyrite crystals. Schoonen and Barnes (1991b) found that pyrite formed from solutions with pH between 2 and 8 was attracted to a hand magnet, suggesting that greigite was also present in the experimental products and was a precursor to pyrite.

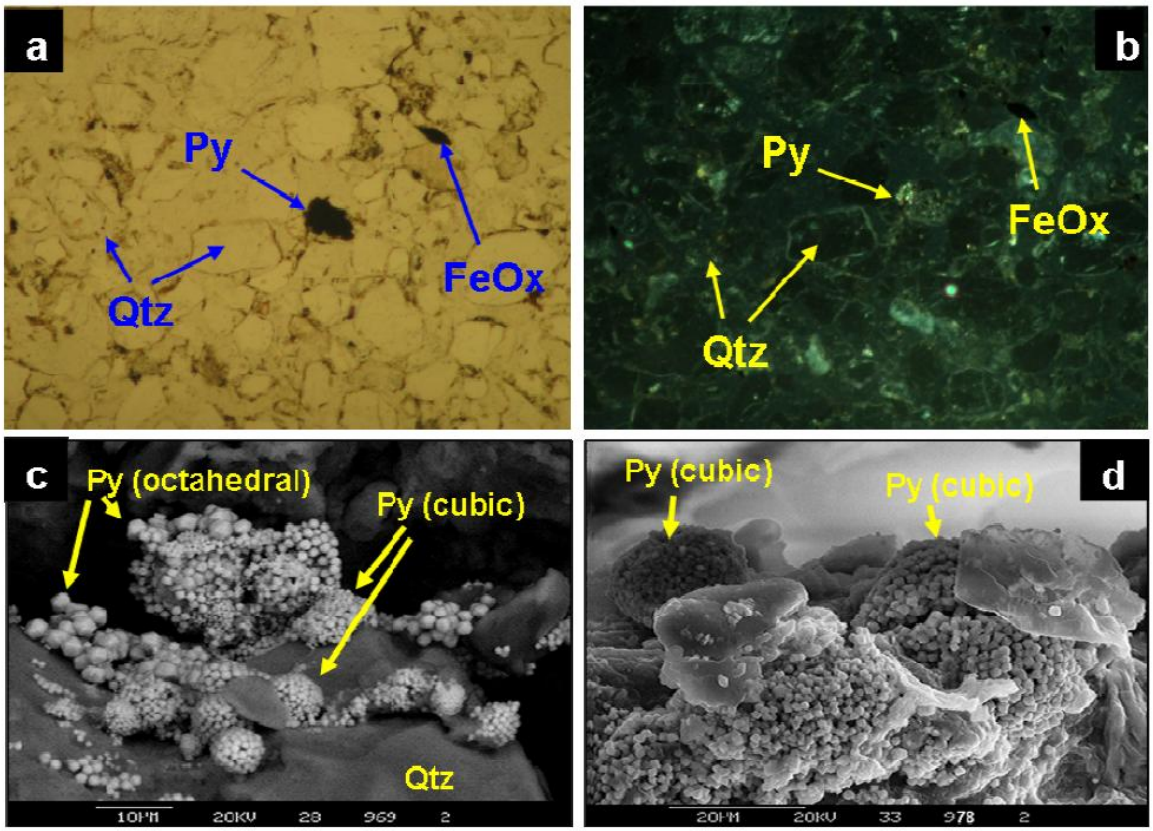

Figure 11-14 Profile BG 11: (a) and (b) thin section photographs from soil profile BG 11, horizon 4Bjg5 showing a cluster of pyrite framboids in a quartz matrix. Frame (a) was viewed under plane polarised light and (b) under reflected light. The field of view indicates scale and was 2.5 mm in (a) and (b). SEM photomicrographs (c) and (d) of rough-surfaced soil samples from the sulfuric 4Bjg4 horizon (100 to 160 cm depth) of profile BG 11. (c) BSE and (d) SE images showing framboidal pyrite and non-framboidal pyrite occurring as clusters within a quartz matrix. The large framboid has layers with different crystal sizes, representing different chemical conditions during formation. The field of view indicates scale and is 75 µm across in (c); 90 µm across in (d). (FeOx: iron oxide, Gy: gypsum, Py: pyrite, Qtz: quartz).

The main macro- and micromorphological characteristics of profile BG 11 are summarised in Figure 11-15. A full description of profile BG 11 micromorphology is provided in Table 11-3.

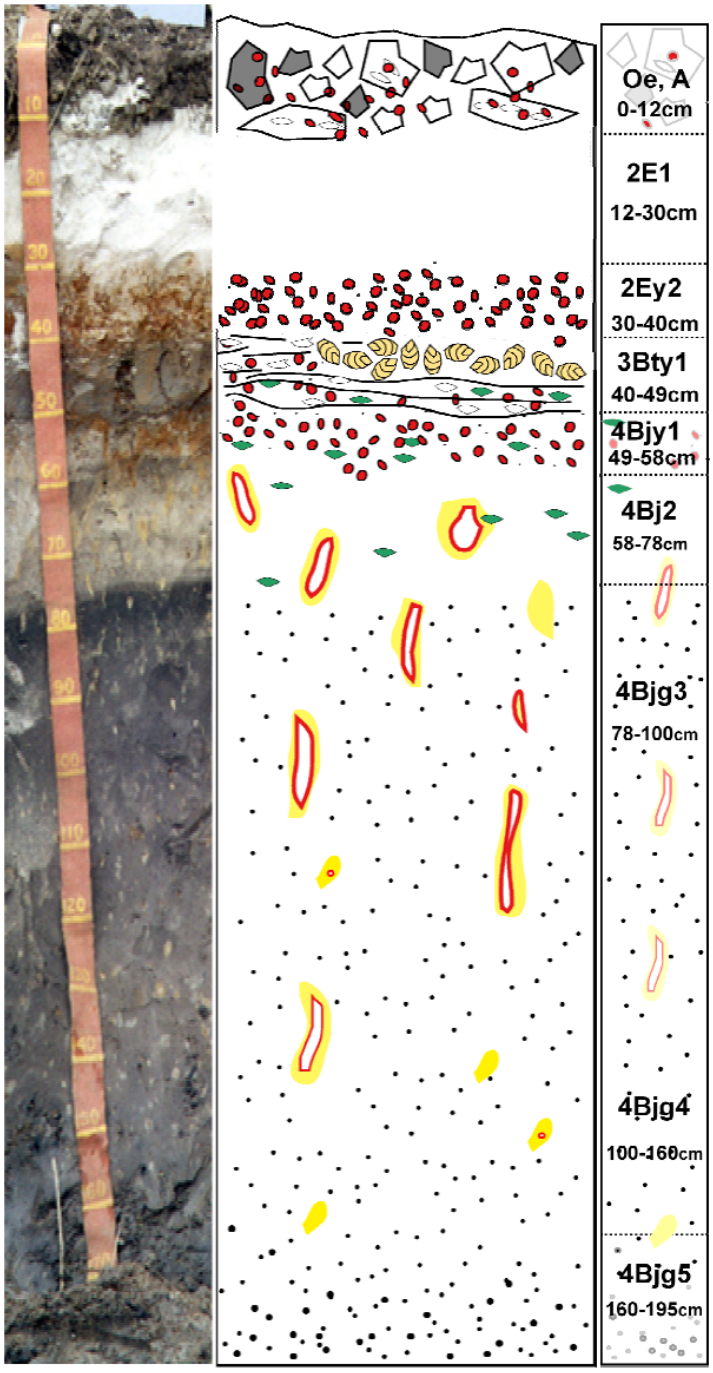

Micromorphology:
Oe, A: Crumb structure, calcareous and siliceous, partly layered with lenticular voids, rounded sand-size iron nodules, not related to pores. Ferrihydrite-goethite nodules are pseudomorphs after pyrite framboids.

2E1: Quartz sand, very little organic residue. Very fine clay coatings on sands, micro laminated.

2Ey2: Sand with strong impregnations of Fe oxides (goethite) associated with blackened organic matter (hemic), pseudomorphs after pyrite. Discontinuous shell lenses with gypsum on the shell surface.

3Bty1: Layered clay, with lenticular voids, showing porostriation. Gypsum crystals (pseudohexagonal and lenticular) as infillings and intercalations, granostriated b-fabric. Few jarosite hypocoatings.

4Bjy1: Sand with gypsum and jarosite hypocoatings around roots, iron coatings and quasicoatings on jarosite. Loose discontinuous infillings of lenticular gypsum, decreasing with depth. Horizontal intercalations of blackened organic matter and black pseudomorphs of pyrite. Coarse lenticular pores (mangrove pneumatophores).

4Bj2, 4Bjg3 and **4Bjg4:** Sulfuric material and pyrite-containing material. Occasionally jarosite coatings form around large root channels, adjacent to root residues. Hypo- and quasicoatings of Fe-oxides on jarosite hypocoatings. Few pyrite framboids scattered in the groundmass.

4Bjg5, 4Bg6: Sulfidic material (pyrite framboids).

Figure 11-15 Main macro- and micromorphological features of profile BG11. Groundwater height fluctuated seasonally between 140 cm and 180 cm during June 2002 to June 2004.

Table 11-2 Micromorphological descriptions of St Kilda profiles (OIL: oblique incident light, PPL: plane polarized light, XPL: crossed polarisers, OM: organic matter).

Profile	Horizon	Microstructure	Porosity	Pedofeatures and Mineral component	Organic components (% in volume, referred to the total organic matter)
600	**Oe1 Depth: 0-12 cm**	Apedal due to abundance of organic tissues, granular in areas richer in amorphous organic matter (OM), moderately separated, granules of medium sand size.	• 80%, mainly packing pores of organic residues and organic material, up to several cm long (65%); some planar voids in polymorphic organic material, fine sand size, accommodated (5%); compound packing voids and star-shaped vughs due to welding of amorphous OM aggregates (10%).	Very fine sand of quartz, equant, angular, fresh, <2% of the volume.	• 30%. Root and leaf residues, from 0.25 mm to several cm, brown, partly anisotropic (XPL) and with a silver lustre (OIL) due to cellulose in fresh cell walls, some of the cells contain phlobaphene. They present different degrees of comminution and blackening, generally starting in the inner parts. Light yellow with oblique incident light. • 50%. Gel-like polymorphic amorphous OM, yellowish grey, dotted or limpid, isotropic, without reflection (OIL), aggregated into granules of very coarse and coarse sand size, moderately welded, or into subangular peds, some of them with internal fissures, containing punctuations of black polymorphic organic material. It also occurs as impregnative coatings of the organic residues. • 20%. Black polymorphic amorphous organic material derived from highly decomposed OM, as very fine sand punctuations, amorphous masses and pore coatings, opaque, isotropic, bright yellow (OIL).
	Oe2 Depth: 12-32 cm	Granular in areas richer in amorphous OM, moderately separated, granules of medium sand size.	• 80%, packing pores of organic residues and organic material, up to several cm long (30%); some planar voids in polymorphic organic material, fine sand size, accommodated (5%); compound packing voids and star-shaped vughs due to welding of amorphous OM aggregates (45%).	Very fine sand of quartz, equant, angular, fresh, <2% of the volume.	• 10%. Root and leaf residues, from 0.25 mm to 1 cm, brown, partly anisotropic (XPL) and with a silver lustre (OIL) due to cellulose in fresh cell walls, some of the cells contain phlobaphene. They present different degrees of comminution and blackening, generally starting in the inner parts, more blackened than the overlying horizon. Light yellow with oblique incident light. • 75%. Gel-like polymorphic amorphous OM, yellowish grey, dotted or limpid, isotropic, without reflection (OIL), aggregated into granules of very coarse and coarse sand size, moderately welded, or into subangular peds, some of them with internal fissures, containing frequent punctuations of black polymorphic organic material. It also occurs as impregnative coatings of the organic residues. • 15%. Black polymorphic amorphous organic material derived from highly decomposed OM, as very fine sand and silt punctuations and as amorphous masses and coatings, opaque, isotropic, bright yellow (OIL).
2610	**Oe1 Depth: 0-8 cm**	Granular in areas richer in amorphous OM, moderately separated, granules of medium sand size.	• 65%, packing pores of organic residues and organic material, up to 1 cm long (20%); some planar voids in polymorphic organic material, fine sand size, accommodated (5%); compound packing voids, star-shape vughs due to welding of amorphous OM aggregates (45%).	Very fine sand of quartz, equant, angular, fresh, <2% of the volume.	• 25%. Root and leaf residues, from 0.25 mm to 1 cm, brown, some of them anisotropic (XPL) and with a silver lustre (OIL) due to cellulose in fresh cell walls, some of the cells contain phlobaphene. Many of them are horizontally oriented. They present different degrees of comminution and blackening, generally starting in the inner parts. Light yellow with oblique incident light. • 60%. Gel-like polymorphic amorphous OM, yellowish grey, dotted or limpid, isotropic, without reflection (OIL), aggregated into granules of very coarse and coarse sand size, moderately welded, or into subangular peds, some of them with internal fissures, containing punctuations of black polymorphic organic material. It also occurs as impregnative coatings of the organic residues. • 15%. Black polymorphic amorphous organic material derived from highly decomposed OM, as very fine sand and silt punctuations and as amorphous masses and pore coatings, opaque, isotropic, bright yellow (OIL).
	Oa2/W1 Depth: 8-30 cm	Layered distribution of the organic material, with a coarse vertical root in the vertical section.	• 50%, horizontal planar voids, unaccommodated, 0.5 to 2 mm, (40%) and vughs and vesicles, coarse sand size, (10%)	Very fine sand of quartz, equant, angular, fresh, <2% of volume. Common pyrite framboids, very fine sand to silt, near the edges of yellow gel, opaque, bright grey (OIL)	• 20%. Root and leaf residues, from 0.25 mm to 1 cm, brown, horizontal, some of them anisotropic (XPL) and with a silver lustre (OIL) due to cellulose in fresh cell walls. Some of the cells contain phlobaphene. They present different degrees of comminution and blackening, generally starting in the inner parts. • 70%. Gel-like polymorphic amorphous OM, yellowish grey, dotted or limpid, isotropic, without reflection (OIL), distributed in layers, with horizontal orange intercalations (probably phlobaphenized organic remains), also aggregated into granules of very coarse and coarse sand size, moderately welded, or into subangular peds, some of them with internal fissures, containing punctuations of black polymorphic organic material. It also occurs as impregnative coatings of the organic residues. • 10%. Black polymorphic amorphous organic material derived from highly decomposed organic matter, irregularly distributed in masses of centimetre size, isotropic, bright yellow with OIL, often included into the yellowish amorphous organic matter, but also as coatings.

Table 11-3 Micromorphological descriptions of profile BG 11 at the Gillman study site (OIL: oblique incident light, PPL: plane polarized light, XPL: crossed polarisers).

Horizon	Micro-structure	Porosity	Coarse mineral elements	Micromass	Organic components	Pedofeatures
Oe – A Depth: 0-12 cm	Crumb, very coarse sand size to 0.5 cm in diameter, strong (highly separated); locally platy.	50%. Compound packing pores, very coarse sand size, 40%; planar and lenticular voids, fine sand size, horizontal within elongated aggregates, 5%; vughs, vesicles and biopores, fine sand size, 5%. In the lower part of the horizon porosity is lower (30%), and structure is fine blocky.	Fine sand of quartz, equant, subrounded, fresh, in clusters; few shell fragments	80% of the aggregates are yellowish grey, dotted, with horizontal fissures, mosaic speckled b-fabric (non calcareous). The rest (20%) are grey, dotted, crystallitic b-fabric (calcareous).	• root sections, moderately well preserved • plant tissues, broken by fauna, some of them blackened. • organic pigment as dots and intercalations in non-calcareous aggregates.	• Some impregnative hypocoatings of micrite in non-calcareous aggregates. • Impregnative red nodules of hematite (OIL) up to 0.5 cm, irregular, around pores in non-calcareous aggregates. • Nodules of Fe oxides (possibly hematite), fine and medium sand, rounded, probably pseudomorphs after pyrite framboids, with a faint halo, showing granostriation, without any relation to pores. • Frequent passage features due to fauna.
2E1 Depth: 12-30 cm	Apedal, single grain.	35 to 40%, simple packing pores, medium sand size.	Quartz (fresh) and few plagioclases and microclines (dotted), equant, subangular, with a bimodal distribution: 80% fine subangular sand, 20% coarse subrounded sand, random distribution.	Absent	• Few tissue residues (hemic)	• Few horizontal intercalations and nodules of grey clay and silt, impregnating the sand, impure, dotted, mosaic-speckled b-fabric. • Very fine clay coatings on sands, microlaminated. • Passage features by burrowing animals
2Ey2 Depth 30-40 cm	Apedal, single grain.	20 to 30%, simple packing pores, medium sand size. 5%. Planar voids, vertical, 0.25 - 0.5 cm thick root channels	Quartz, medium to fine sand, subangular, fresh, random.	Mixture of clay and sand	• Some tissue residues (hemic)	• Areas with very fine clay coatings (10 µm thick) around quartz grains. • Few impregnative intercalations of yellowish-grey mixture of clay and fine silt, mosaic-speckled. • Few impregnative irregular red nodules of clay and iron oxides (OIL) • In the lower half frequent dull-reddish brown impregnations and coatings on quartz grains, as hypocoatings of channels containing blackened organic residues. Fe-oxides as stains and as pseudomorphs after pyrite framboids, 50 µm in diameter.
3Bty1 Depth: 40-49 cm	Platy in the deeper part, blocks with platy aggregates in the upper part, mixed with sand.	20%. Planar voids, horizontal, thickness of very coarse sand size, non accommodated, 10%; vesicles and vughs, medium sand size, 5%; lenticular horizontal pores, coarse sand size, pseudomorphs after gypsum crystals.	Clay with fine quartz sand, subangular, fresh, random.	Light brown mixture of clay and fine silt, speckled. b-fabric: Stipple-speckled and parallel striated (horizontal).	• Blackened layered organic residues and few yellow organic tissue residues, layered.	• Frequent dull-reddish brown impregnations and coatings on quartz grains, as hypocoatings of channels, containing blackened organic residues. Fe-oxides as stains and as pseudomorphs after pyrite framboids, 50 µm in diameter. • Intercalations of strongly blackened pseudomorphs of Fe-oxides after organic residues and pyrite framboids, scattered in the clay and in clusters. • Hypocoatings of Fe oxides around blackened organic residues. • Frequent gypsum crystals in the clay, medium sand, pseudohexagonal and lenticular sections, showing granostriation. • Few jarosite hypocoatings.
4Bjy1 Depth: 49-58 cm	Platy, strong.	40%. Planar voids, horizontal, 0.25 - 0.5 cm thick, non accommodated and lozenge-shaped 20%; Lenticular pores, coarse and very coarse sand size, 10%; faunal pores, vertical, 2 mm thick, 5%; vughs and vesicles, medium sand, 5%.	Quartz, fine sand, subangular, fresh, in clusters and lenses, 5%; gypsum, very coarse sand, pseudohexagonal, rhombohedral and lenticular, in clusters and lenses, 10%; quartz and mica flakes, very fine sand and coarse silt, at random, 5%.	Mixture of clay and fine silt, light brown, speckled. b-fabric: Stipple speckled and occasionally gypsum-striated.	• Horizontal intercalations of blackened organic matter including black pseudomorphs of pyrite. • Yellow organic tissues around biopores.	• Hypocoatings of jarosite, up to 3 mm thick, around faunal pores and aged organic residues. Some of them have intercalations of gypsum sand, hexagonal and pseudohexagonal sections • Fe-oxides coatings and quasicoatings on some of the jarosite hypocoatings. • Loose discontinuous infillings of lenticular gypsum.
4Bj2 Depth: 58-78 cm	Platy, weakly developed.	45%. Simple packing pores, medium and coarse sand size, 35%; channels, vertical, 5 mm thick; planar, horizontal, non accommodated, 2 mm thick, 5%.	Quartz, medium and coarse sand, subangular, fresh, in clusters and lenses, 40%; very coarse sand, pseudohexagonal and lenticular, in clusters and lenses, 10%; quartz and mica flakes, very fine sand and coarse silt, at random, 5%.	Almost absent, as intercalations and impregnations of non-calcareous mixture of clay and fine silt, with a stipple-speckled b-fabric.	• Blackened organic tissue residues including black pseudomorphs of pyrite. • Yellow organic tissues around biopores.	• Impregnations of jarosite, as nodules and hypocoatings in coarse pores, up to 1 cm thick. • Hypo and quasi-coatings of Fe-oxides (red under OIL), on jarosite hypocoatings. • Very fine clay coatings on quartz grains.
4Bjg3 Depth: 78-100 cm	Single grain structure	30%. Simple packing pores, medium sand, 25%; root channels, 3 to 5 mm thick, 5%.	Quartz, microclines and plagioclases, fresh, medium and coarse sand size, subangular, moderately sorted.	Almost absent, as intercalations and impregnations of non-calcareous mixture of clay and fine silt, with a stipple-speckled b-fabric.	• Light brown root and tissue residues, anisotropic. • Charcoal fragments, well preserved. • Amorphous opaque organic punctuations	• Coatings and impregnative hypocoatings of jarosite on channel walls, 1 to 2 mm thick, diffuse boundaries. • Infillings of jarosite between horizontal plant tissue residues, dense discontinuous. • Hypo and quasi-coatings of Fe-oxides (red under OIL), on jarosite hypocoatings. • Few pyrite framboids scattered in the groundmass. • Fine amorphous silica coatings on quartz grains.
4Bjg4 andg 4Bjg5 Depth: 100-195 cm	Single grain structure	30%. Simple packing pores, medium sand, 25%; root channels, 3 - 5 mm thick, 5%.	Quartz, microclines and plagioclases, fresh, bimodal distribution of sizes: medium sand, subangular and coarse sand, subrounded.	Grey clay and fine silt, stipple speckled b-fabric, aggregated into very fine sand granules.	• Light brown root and tissue residues, anisotropic. • Charcoal fragments, well preserved. • Amorphous opaque organic punctuations.	• Frequent pyrite framboids, 50 µm in diameter, scattered in the groundmass and as clusters • Fragments of pyrite with polygonal sections • Large tissue residue with an internal coating and impregnative hypocoating of jarosite, 1 to 2 mm thick. The layers of the tissue adjacent to the groundmass have pyrite framboids on channel walls, while the ones near the pore have hypocoatings of Fe oxides. • Fine amorphous silica coatings on quartz grains.

11.6. Conceptual model for oxidation of an acid sulfate soil

Soil profiles at Gillman (e.g. profile BG 11) have had a complex geomorphic and drainage history. The loss of tidal flooding in 1935 caused: **(i)** oxidation of hyposulfidic materials in the upper portion of the soil profile, **(ii)** oxidation of hypersulfidic materials in the lower portion of the soil profile, which developed sulfuric materials that led to the acidification of groundwater, and **(iii)** reduction of Fe and S during seasonal re-flooding of the lower portion of soil profiles. The development of redoximorphic features that were commonly observed in soil profiles containing acid sulfate soil materials at Gillman are explained by Figure 11-16. The figure shows a schematic cross-section of a macro pore (void) site, formed during the decomposition of a mangrove root. The different slides in Figure 11-16 describe the mineral transformations that may occurred in different acid sulfate soil materials during oxidation and re-flooding scenarios.

Development of redoximorphic features and mineral transformations within:

i. **hyposulfidic materials** in the upper portion of the profile oxidised in circum-neutral conditions. Pyrite occurred in the matrix associated with organic matter. The high pH caused iron oxides to precipitate locally, replacing pyrite structures as iron oxide pseudomorphs. Jarosite may have formed in acidic micro-environments between pyrite crystals in framboids to form box-work structures and pitted crystal faces. Jarosite was subsequently replaced by iron oxide. Calcium availability and high pH caused gypsum to crystallise as rhombohedral and prismatic forms, which were largely leached out of the upper portion of the profile by infiltration of meteoric waters, leaving characteristically shaped voids (Figure 11-16; 1a, 1b and 1c).
ii. **hypersulfidic materials** occurred deeper in the soil profile where sandy soils had less buffering capacity. Pyrite originally occurred as large framboids and large crystals that occurred scattered in the matrix and concentrated around decomposed mangrove pneumatophores (Figure 11-16; 2a). Pyrite oxidation caused soil acidification (pH<4) which caused jarosite to precipitate as thin hypocoatings that impregnated the matrix and partially infilled pores. Fe-oxides formed thin films on exposed surfaces of jarosite structures (Figure 11-16; 2b). Infiltration of meteoric waters containing carbonate increased soil pH in some areas which allowed

jarosite to progressively transform to goethite, and gypsum to precipitate as lenticular prisms (Figure 11-16; 2c).

iii. **reflooding** (seasonally) of the lower portion of the profile caused Eh to drop as microbes reduced sulfate to sulfides in areas containing organic matter, consuming acidity and locally raising soil pH. The rise in pH caused jarosite to further transform to goethite on structural surfaces. Formation of small pyrite crystals and framboids occurred in strongly reduced micro-environments in the macro-pore or as small diffuse, black concentrations (redoximorphic features) in the matrix (Figure 11-16 3a and 3b).

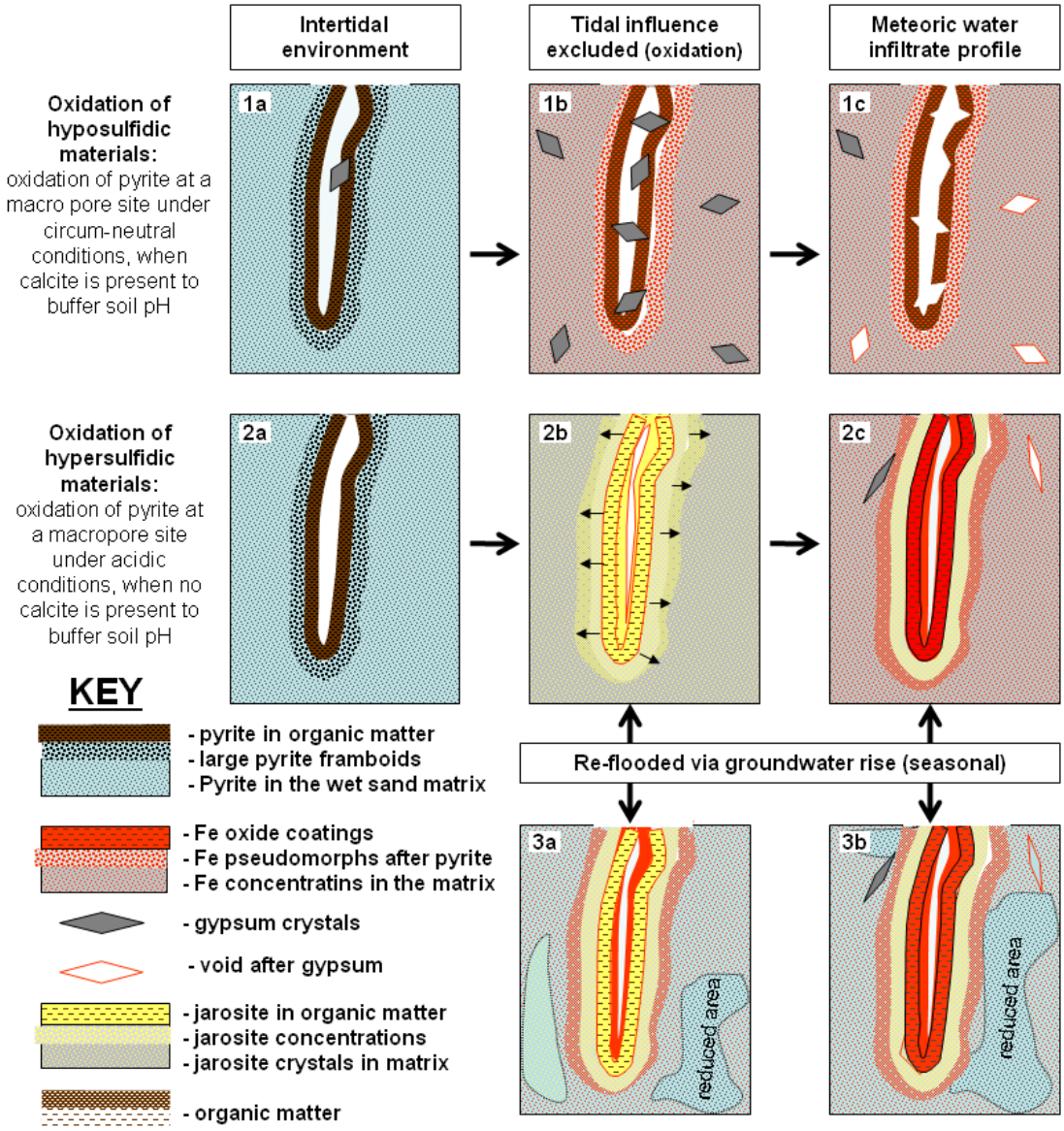

Figure 11-16 Schematic diagram showing mineral transformations that occurred under changed hydraulic conditions within a macropores (mangrove root channel) from the sandy soil layers of profile BG 11. Individual frame widths provide scale (measuring about 1.5 cm across).

11.7. Summary

In this chapter, soil micromorphology and scanning electron microscopy (SEM) were used to describe and characterise the imprints of biological, physical, chemical and mineralogical processes within two intertidal soils and one drained supratidal soil profile (BG 11). These techniques were used to:

(i) define the various types of organic matter fractions (i.e. sapric, hemic, fibric materials),

(ii) describe the occurrence of sulfide minerals (e.g. pyrite, monosulfides and chalcopyrite) and

(iii) describe micro-scale weathering pathways and mechanisms under changing hydrological, physical and biogeochemical conditions.

The micromorphology of these soils provided an insight to, and confirmed at a detailed scale, the processes that contributed to their formation in a reduced environment and their alteration during oxidation. In the intertidal (undrained) mangrove soils at St Kilda, the micromorphology of organic material indicated that sapric material was more decomposed, less porous and allowed the formation of larger pyrite framboids than hemic material. In these Hydrosols, partial oxidation of pyrite along coarse pores formed lenticular gypsum because of the presence of calcium in the environment. The morphology and form of pyrite and gypsum crystals indicated that the conditions of their formation were on a micrometre-scale.

Sulfide oxidation was extensive in the drained soil at Gillman, evidenced by the formation of iron oxyhydroxide pseudomorphs (goethite crystallites and framboids) after pyrite, jarosite and gypsum crystals. The morphology and relationships of pseudomorphs after pyrite formation can be used as a palaeo-indicator of the soil's physio-chemical conditions prior to oxidation.

The micromorphology of weathering features of pyrite crystals, framboids and mottles provided insight into the pH and redox conditions (i.e. within micro-environments) and weathering rates as oxidation proceeded. Iron oxide pseudomorphs after jarosite

spheroids within salt efflorescences also indicated dynamic oxidising micro-environments.

The preservation of pyrite crystals within drained soils at Gillman occurred by armouring with clay coatings and by impregnation or inclusion within gypsum and halite crystals, and has implications for characterisation of acid sulfate soil types by ageing as well as for their management.